JOURNAL OF GEOPHYSICAL RESEARCH, VOL. 101, NO. C8, PAGES 18,043–18,059, AUGUST 15, 1996

The influence of canyons on shelf currents: A theoretical study

Xiaoyang Chen and Susan E. Allen

Department of Earth and Ocean Sciences, University of British Columbia, Vancouver, Canada

Abstract. The influence of submarine canyons on shelf currents is studied using the Rossby adjustment method for a homogeneous, inviscid fluid on an f plane. The canyon in the model is assumed to have vertical edges and constant width. The geostrophic flow around a canyon is found to be dependent upon two geometric parameters: the ratio of the depth of the canyon to the depth of the shelf and the ratio of the width of the canyon to the Rossby radius over the canyon. Moreover, a single parameter determines most of the properties of the geostrophic state. This parameter is called the canyon number and is a combination of the two basic geometric parameters. In the geostrophic state an infinitely long flat-bottom canyon will act as a complete barrier to an approaching shelf flow. The approaching flow is asymmetrically diverted along the canyon, and a net flux is generated to the left of the flow in the northern hemisphere. If the canyon cuts a shelf between the shelf break and the coast and connects to a strait (the geometry of Juan de Fuca Canyon) an in-canyon (out-canyon) current will be generated when the shelf break current flows keeping the shelf at its left (right) in the northern hemisphere. If the canyon has a stepped or sloped bottom, the geostrophic flow has a singularity where the step or slope meets the left canyon edge (looking upcanyon) in the northern hemisphere. Flow can cross the canyon edge through the singularity, so the canyon is no longer a complete barrier to the approaching shelf flow. In this case, as above, a net flux is generated to the left of the approaching shelf flow.

1. Introduction

Submarine canyons are one of the main topographic features of the coastal regions of the world's oceans. Observations have shown that a canyon may have very important effects on the local circulation. Many observational studies in the past focused on tides or internal waves and the effects of these relatively high frequency currents on sediment distribution and resuspension in canyons [*Drake et al.*, 1978; *Gordon and Marshall*, 1976; *Hotchkiss and Wunsch*, 1982; *Inman et al.*, 1976; *Keller et al.*, 1973; *Keller and Shepard*, 1978; *Shepard et al.*, 1979]. The study of longer-timescale (and time mean) currents in and around submarine canyons started in the early 1980's with *Han et al.* [1980] and *Freeland and Denman* [1982].

Han et al. [1980] found that the velocities at the bottom near the Hudson Shelf Valley were clearly aligned with the canyon topography. *Freeland and Denman* [1982] and *Freeland et al.* [1984] presented observations over the continental shelf near Vancouver Island that showed a persistent deflection of the summer coastal flow near a small submarine canyon in this region. *Hickey et al.* [1986] described multiyear observations of currents and suspended sediments in Quinault Canyon. Their observations revealed a correlation between flow along the canyon axis and the along-shelf circulation; the pressure gradient due to the geostrophically balanced coastal flow forces upwelling or downwelling in the deep parts of the canyon. *Hunkins* [1988] analyzed a set of approximately yearlong current measurements near the head of and in Baltimore Canyon that show the existence of persistent upcanyon and downcanyon flows. Currents near the surface are not strongly affected by the submarine canyon; however, currents at the bottom seem to align with the canyon isobaths. All of these observational studies support the existence of coupling between shelf and canyon circulation. This coupling exists both in shallow shelf-canyon systems (e.g., Hudson Shelf Valley [*Mayer et al.*, 1982]) and in deep ones (e.g., Juan de Fuca Canyon [*Freeland and Denman*, 1982]).

Several efforts have been made to construct theoretical models to explain the dynamics of the coupling between shelf and canyon circulation. *Freeland and Denman* [1982] proposed that the currents within a narrow canyon are forced by the unbalanced pressure gradient, which is supplied by the geostrophic shelf flow just above the top of the canyon. In their theoretical model, the shelf-canyon interaction allows water to be raised from depths much greater than that normally expected from the classical wind-driven upwelling mechanism. Their calculations correspond reasonably well with their observations. However, their theory neglected the transverse velocity and hence the Coriolis effect within the canyon, limiting its validity to canyons much narrower than the Rossby radius.

The geostrophic adjustment of a stratified coastal current in the presence of an infinitely long, rectangular, flat-bottom canyon is considered by *Klinck* [1988, 1989]. His model includes the feedback of the upwelled dense water on the cross-shelf pressure gradient, which was not considered in the model of *Freeland and Denman* [1982]. In *Klinck's* model, the initial flow on the shelf is assumed to be geostrophic and barotropic with trigonometric dependence in the along-canyon direction. For each vertical mode the decay scale of the perturbation is determined by a scale that is the shorter of the radius of deformation for that mode and the width of the coastal current. The width of the canyon determines the strength of the cross-canyon flow and thus the strength of the canyon's effect on the

Page number 96JC01149.
0148-0227/96/96JC-01149$09.00

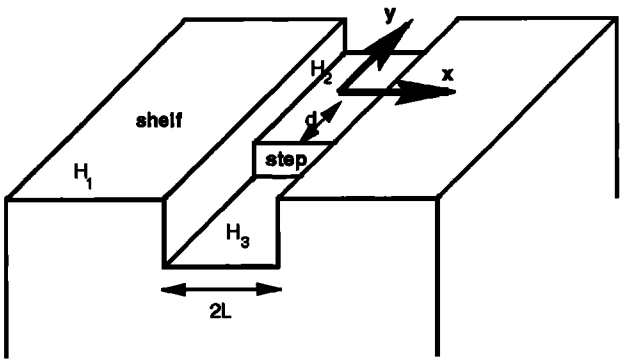

Figure 1. The geometry of the stepped-bottom canyon model. The canyon has vertical walls and is infinitely long. The shelf is flat and infinitely wide with depth H_1. The canyon bottom is divided by a step into two portions: a shallow upper canyon portion with depth H_2 and a deep lower canyon portion with depth H_3. Here x is in the cross-canyon direction, and y is along the central axis of the canyon. The step is at $y=d$.

overlying coastal current, with the interaction becoming smaller as the canyon width becomes smaller than the current width or the radius of deformation. Even in the case of flow over a narrow canyon, the isopycnals at the top of the canyon are distorted, and there is also some residual circulation on the shelf forced by the presence of the canyon.

It is tempting to seek a steady state for the interaction between shelf and canyon circulation. One of the possible approaches is to use Rossby adjustment to derive the steady state solution and avoid the relatively complicated, transient initial value problem. One purpose of our study is to apply this approach to investigate the basic dynamics in the interactive process of a shelf flow and a canyon. For a review of the open ocean adjustment problem, see *Gill* [1982, pp. 191-203]. *Gill et al.* [1986] applied the Rossby adjustment method to study the topographic problem and considered the problem of how a barotropic flow is modified when it passes over a steplike topography, using linear analysis and numerical and laboratory experiments. Extending the work of *Gill et al.* [1986], *Allen* [1988, 1996a] studied Rossby adjustment over a slope.

Since the purpose of our research is to reveal the basic properties of the shelf-canyon interaction and the effect of the canyon shape on the circulation, as a first step this paper will consider a homogeneous, inviscid fluid on an f plane. As will be demonstrated later, a rotating fluid, not initially in equilibrium, adjusts around a canyon to a final geostrophic state through long modified double Kelvin waves which transmit information along the canyon. The geostrophic state will be derived by constructing the solution from these long "canyon waves." The transient, propagating wave solution is investigated numerically by *Chen* [1996].

Three types of canyon geometry, all with vertical walls and constant width, will be considered. The simplest is an infinitely long flat-bottom canyon cutting a flat shelf. Some effects of topography within the canyon will be investigated using an infinitely long canyon with a step dividing it into two sections, one deep and one shallow but both deeper than the shelf. The geometry of this type of canyon is shown in Figure 1. The third canyon geometry is designed to include the main features of Juan de Fuca Canyon. In this case the canyon cuts through a flat shelf, the mouth of the canyon is at the shelf break, and the head of the canyon connects with a strait. The bottom of the canyon consists of four segments, with two flat regions and two slopes joining them. The geometry of this type of canyon is shown in Figure 2. The coordinates used in this paper are oriented with x in the across-canyon direction and y along the central axis of the canyon.

The governing equations will be given in next section. The properties of the double Kelvin waves that exist in a flat-bottom canyon will be discussed in section 3. To provide the foundation for this paper, the geostrophic circulation over a flat-bottom canyon will be described in section 4. The far-field solution will be found by constructing a solution of long canyon waves. This solution will be demonstrated, in the case of a specified initial condition in which the fluid is at rest but in which there is a surface discontinuity, to be the geostrophic solution for a flat-bottom canyon in the far-field. An important parameter, σ, will be defined in the process of solving

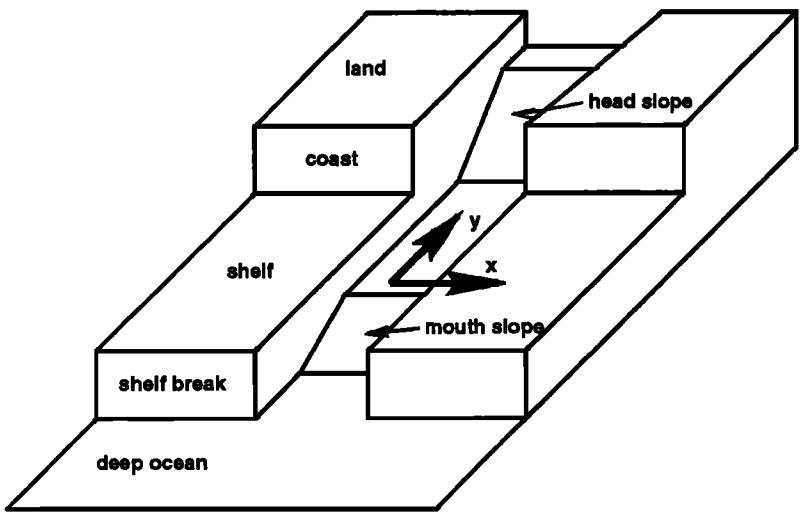

Figure 2. The geometry of the Juan de Fuca Canyon model. The bottom of the canyon consists of four segments: deep mouth part, mouth slope, main body, and head slope; the edges are vertical, and the width is constant. The shelf break, coast, and strait walls are all vertical. The length of the strait is infinite. The shelf is infinitely long and is flat.

the problem. The flux and the full solution will be calculated under the special initial condition. By applying the solutions obtained in section 4, discussion of the geostrophic state around a stepped-bottom canyon will be presented in section 5. Effects of the shelf break, coast, and strait on the circulation around a canyon will be studied in section 6. A discussion will be given in section 7, and the conclusions will be presented in section 8.

2. Governing Equations

In a homogeneous, inviscid fluid on an f plane the governing equations for small disturbances are the linear shallow water equations,

$$\frac{\partial u}{\partial t} - fv + g\frac{\partial \eta}{\partial x} = 0, \tag{1a}$$

$$\frac{\partial v}{\partial t} + fu + g\frac{\partial \eta}{\partial y} = 0, \tag{1b}$$

$$\frac{\partial \eta}{\partial t} + \frac{\partial}{\partial x}(Hu) + \frac{\partial}{\partial y}(Hv) = 0, \tag{1c}$$

where f is the Coriolis parameter, g is the acceleration due to (possibly reduced) gravity, H the undisturbed depth of the fluid, and $\mathbf{u} = (u, v)$ the horizontal velocity of the fluid. The coordinates are defined in section 1.

The depth in all our canyon models is constant except at the canyon edges, the shelf break, and the canyon slopes. In all other regions the gradient of the topography, ∇H, is zero. Therefore introduce an initial quantity

$$Q_I(x,y) = \frac{H}{f}\zeta_I(y) - \eta_I(y), \tag{2}$$

where $\zeta = \partial v/\partial x - \partial u/\partial y$ is the relative vorticity and the subscript I denotes a variable at the initial time t=0 and where we have assumed the initial conditions are independent of x. Manipulating (1) gives an equation for η alone in terms of this initial quantity

$$\left(\frac{1}{f^2}\frac{\partial^2}{\partial t^2} - R^2\nabla^2 + 1\right)\eta(x,y,t) = Q_I(x,y), \tag{3}$$

where $R = (gH)^{1/2}/f$ is the barotropic Rossby radius of deformation.

Solution of this initial value problem (3) can be found by adding a particular solution of it, which is the steady solution $\eta_s(x,y)$, given by

$$R^2\nabla^2\eta_s(x,y) - \eta_s(x,y) = Q_I(x,y) \tag{4}$$

to the solution of the homogeneous equation, which is the transient wave solution $\eta_w(x,y,t)$, given by

$$\left(\frac{1}{f^2}\frac{\partial^2}{\partial t^2} - R^2\nabla^2 + 1\right)\eta_w(x,y,t) = 0, \tag{5}$$

and with the initial condition $\eta_w(x,y,0) = -Q_I(x,y) = -\eta_s(x,y)$.

Equation (4) can be solved only after the values of η_s at the edges of the piecewise composed domain have been determined; these are the boundary conditions for (4).

A property of the boundary conditions for (4) can be obtained by combining (1) and assuming a steady state,

$$\mathbf{u}_s \cdot \nabla H = 0.$$

Thus geostrophic currents, $\mathbf{u}_s$, must be parallel to the canyon walls, the canyon bottom step or slope, and the shelf break since at these locations $\nabla H \neq 0$. The combination of requiring no flow across the canyon edges and along the canyon over the canyon bottom slope implies that there is no flow over the canyon bottom slopes. Geostrophic flows cannot cross these changes in depth (except at their intersections). This requirement means that η_s is a constant along the edge of each piecewise segment of the domain. We will use this property later to determine the boundary conditions for (4).

3. Canyon Waves

Instead of solving the complete time dependent problem (5) in this section, we present an analysis of the properties of canyon waves and of the structure of long canyon waves. Since the purpose of this paper is to present the geostrophic circulation, i.e., the solution of (4), the transient solution of (3) will be deferred to a later paper.

Consider an infinitely long canyon with vertical walls and a constant depth H_2; the width of the canyon is a constant $2L$, and the depth of the shelf is a constant H_1 ($H_1 \neq H_2$). Assume that the solution of (5) takes a wavelike form

$$\eta_w(x,y,t) = E(x)\exp[i(ky - \omega t)], \tag{6}$$

where $E(x)$ is a function of x, $\omega > 0$ is the frequency, and k is the wave number in the along-canyon direction. Substituting (6) into the momentum equations (1a) and (1b) gives

$$u_w(x,y,t) = i\frac{g[\omega E' - fkE]}{f^2 - \omega^2}\exp[i(ky - \omega t)], \tag{7}$$

$$v_w(x,y,t) = \frac{g[fE' - \omega kE]}{f^2 - \omega^2}\exp[i(ky - \omega t)], \tag{8}$$

where $E'(x)$ is the first derivative of E. Substituting (6) into (5) gives

$$\frac{d^2E}{dx^2} - \alpha_i^2 E = 0, \quad i = 1, 2, \tag{9}$$

where

$$\alpha_i^2(\omega,k) = \frac{f^2 - \omega^2 + k^2gH_i}{gH_i}, \quad i = 1, 2. \tag{10}$$

Because we are looking for waves trapped to the canyon, the parameter α must be real, i.e., $\alpha_i^2 > 0$.

The bounded solution of (9) has the form

$$E = \begin{cases} A_1\exp(\alpha_1 x), & x < -L, \\ A_2\exp(\alpha_2 x) + B_2\exp(-\alpha_2 x), & x < |L|, \\ B_3\exp(-\alpha_1 x), & x > L, \end{cases} \tag{11}$$

where A_1, A_2, B_2 and B_3 are all nonzero constants.

Substituting the form (11) into the equations for η_w and u_w [(6) and (7)], the requirement of continuity of η_w and Hu_w at the canyon edges gives

$$\exp(-\alpha_1 L)A_1 - \exp(-\alpha_2 L)A_2 - \exp(\alpha_2 L)B_2 = 0, \tag{12a}$$

$$H_1(\alpha_1\omega - kf)\exp(-\alpha_1 L)A_1 - H_2(\alpha_2\omega - kf)\exp(-\alpha_2 L)A_2 + H_2(\alpha_2\omega + kf)\exp(\alpha_2 L)B_2 = 0, \tag{12b}$$

$$\exp(\alpha_2 L)A_2 + \exp(-\alpha_2 L)B_2 - \exp(-\alpha_1 L)B_3 = 0, \tag{12c}$$

$$H_2(\alpha_2\omega - kf)\exp(\alpha_2 L)A_2 - H_2(\alpha_2\omega + kf)\exp(-\alpha_2 L)B_2 + H_1(\alpha_1\omega + kf)\exp(-\alpha_1 L)B_3 = 0, \tag{12d}$$

which can be written in matrix form as

$$\mathbf{M}\begin{bmatrix} A_1 \\ A_2 \\ B_2 \\ B_3 \end{bmatrix} = 0.$$

For a nontrivial solution of (12), the determinant $|\mathbf{M}|$ must be zero, which yields the dispersion relation for canyon waves

$$\left(\frac{kf}{\omega}\right)^2\left(\frac{H_2}{H_1}-1\right)^2 = \left(\frac{H_2}{H_1}\right)^2 \alpha_2^2 + \alpha_1^2 + 2\left(\frac{H_2}{H_1}\right)\alpha_1\alpha_2 \coth(2L\alpha_2), \quad (13)$$

where α_1 and α_2 are functions of ω and k as given by (10), and coth( ) is the hyperbolic cotangent function.

The phase and the group speed of canyon waves can be obtained from the dispersion relation (13). Both the phase and the group speed are functions of the wave number, so canyon waves are dispersive. Because the dispersion relation is symmetric about the ω axis, the phase and energy (as well as information) of canyon waves propagate in both directions along the canyon.

The dispersion relation for canyon waves with $\beta = 2L/R_2 = 1$ and $\gamma^2 = H_2/H_1 = 2$, 3, 4, and 5 is given in Figure 3, for $k > 0$. Obviously, for canyon waves, the shorter the wave length is (compared with the Rossby radius over the canyon), the smaller the group speed is (the derivative of the dispersion relation). The limiting cases are as follows:

1. For short waves ($k >> 1/R_2$), the group speed approaches zero.

2. For long waves ($k << 1/R_2$, and so $\omega << f$), (13) gives

$$c_0 = \frac{\omega}{k} = c_1 \frac{|\gamma^2 - 1|}{\left(\gamma^2 + 2\gamma\coth\beta + 1\right)^{1/2}}, \quad (14)$$

where $c_1 = (gH_1)^{1/2}$ is the long-wave phase speed on the shelf. The parameter c_0 is the group speed and phase speed of the long canyon waves. For the infinitely wide canyon limit ($\beta \to \infty$), $c_0 = (gH_2)^{1/2} - (gH_1)^{1/2}$, which is identical to the double Kelvin wave phase speed for a single step found by *Gill et al.* [1986].

Poincare waves (first class waves) are the only waves possible in a barotropic, flat-bottom ocean on an f plane far from lateral boundaries. These waves establish the classic Rossby adjustment [*Gill*, 1982], which will be the solution far from the canyon in our infinitely long canyon models. Note that the final, steady state will differ from the initial condition only in a narrow (one Rossby radius wide) region around the original change in surface elevation. Farther from the initial disturbance the propagating Poincare waves will carry energy but no surface height changes.

The presence of a change in depth allows second-class waves (potential vorticity waves [see *Rhines*, 1969]), of which canyon waves are an example. These waves travel along a depth change and can carry changes of surface elevation over infinitely long distances. Permanent changes over long distances, which determine the steady state, are controlled by long waves. Long Poincare waves have zero group velocity, but long double Kelvin waves have finite group velocity as shown in (14) for the example of long canyon waves.

Canyon waves are dispersive in general; however, long canyon waves are nondispersive, and the group speed ap-

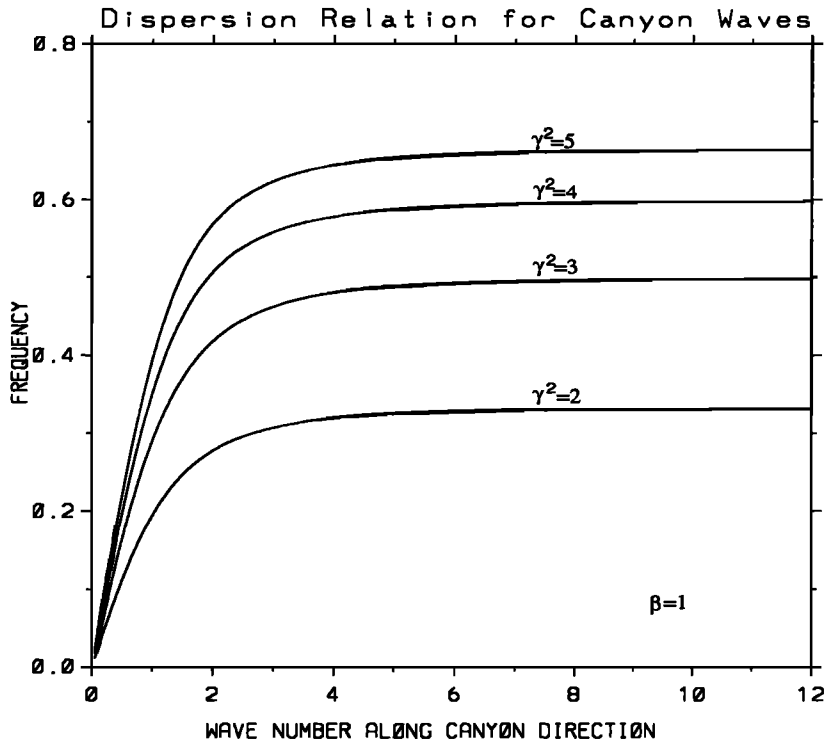

Figure 3. Dispersion relation of canyon waves for the flat-bottom canyon of $\beta = 1$, $\gamma^2 = 2$, 3, 4, and 5. The horizontal axis is the nondimensional wave number along the canyon, kR_2, and the vertical axis is the nondimensional frequency ω/f.

proaches a maximum value that is determined by the geometric parameters of the system. The group speed of short canyon waves approaches zero. These properties of canyon waves will be used in the next section to determine the far-field solution for a flat-bottom canyon.

4. Geostrophic Circulation Over a Flat-Bottom Canyon

4.1. General Far-field Solution

The far-field solution for a flat-bottom canyon will be obtained in this section by constructing the solution as long canyon waves. The Poincare waves are very much in presence but are not explicitly calculated because they are not important to the far-field solution, as was noted in the last section. Using potential vorticity, the solution can be calculated without a full calculation of the time variation. This method is the standard technique of Rossby adjustment [*Gill*, 1982; *Gill et al.*, 1986]. In the far field ($|y| >> R_2$) where the surface is initially flat (i.e., $\eta_I = \text{const}$) assume that the solution of (1) takes the form

$$\eta(x,y,t) = \eta_I(y) - E(x)\exp[i(ky - wt)], \tag{15}$$

where $E(x)$ has the form of (11) with $\alpha_1 = 1/R_1$ and $\alpha_2 = 1/R_2$ for long canyon waves. The corresponding $u(x,y,t)$ and $v(x,y,t)$ are given by (7) and (8), respectively. Now using (15), (7), and (8) to examine the magnitude of each term in the momentum equations, (1a) and (1b), for long canyon waves ($k << 1/R_2$ and $\omega = c_0 k$), we have

$$\left|\frac{\partial u}{\partial t}\right| \approx \frac{g c_0 |c_0 E' - fE|}{f^2} k^2, \tag{16a}$$

$$|fv| \approx g|E'|, \tag{16b}$$

$$\left|g\frac{\partial \eta}{\partial x}\right| = g|E'|, \tag{16c}$$

$$\left|\frac{\partial v}{\partial t}\right| \approx \frac{g c_0 |E'|}{f} k, \tag{17a}$$

$$|fu| \approx \frac{g|c_0 E' - fE|}{f} k, \tag{17b}$$

$$\left|g\frac{\partial \eta}{\partial y}\right| = g|E|k. \tag{17c}$$

The first term of (1a), i.e., (16a), is much smaller than the second and the third ones, i.e., (16b) and (16c), so the first term is negligible in (1a); all terms of (1b), i.e., (17a), (17b) and (17c), are small but of the same order, so all terms must be considered in (1b). For a solution of (1) having the form (15), the momentum equations (1a) and (1b) reduce to

$$-fv + g\frac{\partial \eta}{\partial x} \approx 0, \tag{18a}$$

$$\frac{\partial v}{\partial t} + fu + g\frac{\partial \eta}{\partial y} = 0. \tag{18b}$$

Using (11) for $E(x)$, we write (15) in another form,

$$\eta(x,y,t) = \eta_I - A(y,t)\exp[(x+L)/R_1], \quad x < -L, \tag{19a}$$

$$\eta(x,y,t) = \eta_I - B(y,t)\exp[-(x+L)/R_2] + C(y,t)\exp[(x-L)/R_2], \quad x < |L|, \tag{19b}$$

$$\eta(x,y,t) = \eta_I - D(y,t)\exp[-(x-L)/R_1], \quad x > L, \tag{19c}$$

where A, B, C, and D are functions of two variables and are to be determined. An advantage of assuming that (1) has a solution of the form (19) is that

$$A(y,0) = B(y,0) = C(y,0) = D(y,0) = 0. \tag{20}$$

Substituting (19) into (18a) gives

$$v(x,y,t) = -\frac{g}{f}\frac{A}{R_1}\exp[(x+L)/R_1], \quad x < -L, \tag{21a}$$

$$v(x,y,t) = -\frac{g}{f}\frac{1}{R_2}\left\{-B\exp[-(x+L)/R_2] + C\exp[(x-L)/R_2]\right\}, \quad x < |L|, \tag{21b}$$

$$v(x,y,t) = \frac{g}{f}\frac{D}{R_1}\exp[-(x-L)/R_1], \quad x > L. \tag{21c}$$

Then substituting (19) and (21) into (18b) gives

$$u(x,y,t) = -\frac{g}{f}\left\{\eta_{Iy} - \left(A_y + \frac{A_t}{fR_1}\right)\exp[(x+L)/R_1]\right\}, \quad x < -L,$$

$$u(x,y,t) = -\frac{g}{f}\left\{\eta_{Iy} - \left(B_y - \frac{B_t}{fR_2}\right)\exp[-(x+L)/R_2] - \left(C_y + \frac{C_t}{fR_2}\right)\exp[(x-L)/R_2]\right\}, \quad x < |L|,$$

$$u(x,y,t) = -\frac{g}{f}\left\{\eta_{Iy} - \left(D_y - \frac{D_t}{fR_1}\right)\exp[-(x-L)/R_1]\right\} \quad x > L,$$

where the subscript t denotes a derivative with respect to time and the subscript y denotes a derivative with respect to y.

Using the boundary conditions that the surface elevation and the cross-canyon flux are continuous at the edges of the canyon, we have

At x=-L

$$A = B + C\exp(\beta), \tag{22a}$$

$$H_1\left(\eta_{Iy} - A_y - \frac{1}{fR_1}A_t\right) = H_2\left\{\eta_{Iy} - B_y - C_y\exp(-\beta) - \frac{1}{fR_2}[-B_t + C_t\exp(-\beta)]\right\}, \tag{22b}$$

At x=L

$$B\exp(-\beta) + C = D, \tag{22c}$$

$$H_2\left\{\eta_{Iy} - B_y\exp(-\beta) - C_y - \frac{1}{fR_2}[-B_t\exp(-\beta) + C_t]\right\} = H_1\left(\eta_{Iy} - D_y + \frac{1}{fR_1}D_t\right), \tag{22d}$$

where β, as defined in last section, is the width of the canyon made nondimensional by the Rossby radius over the canyon. If we assume that the surface height is $\eta_L(y,t)$ at the canyon edge $x = L$ and is $\eta_{-L}(y,t)$ at the canyon edge $x = -L$, we have $\eta_{-L} = \eta_I - A$ and $\eta_L = \eta_I - D$. By combining with (22a) and (22c), (19) can also be expressed in another form, in terms of η_L and η_{-L},

$$\eta(x,y,t) = \eta_I + (\eta_{-L} - \eta_I)\exp[(x+L)/R_1], \quad x < -L, \tag{23a}$$

$$\eta(x,y,t) = \eta_I + \frac{1}{2}\left\{(\eta_L + \eta_{-L} - 2\eta_I)\frac{\cosh(x/R_2)}{\cosh(L/R_2)}\right.$$

$$+(\eta_L-\eta_{-L})\frac{\sinh(x/R_2)}{\sinh(L/R_2)}\Big\}, \quad x<|L|, \tag{23b}$$

$$\eta(x,y,t)=\eta_I+(\eta_L-\eta_I)\exp\left[-(x-L)/R_1\right], \quad x>L. \tag{23c}$$

This form of solution will be used later to analyze the geostrophic circulation around the other two canyon models.

Now we have four equations (22) for four unknowns A, B, C, and D. For $f>0$ the procedure to solve the system is given in the appendix. The functions A and D are

$$A(y,t)=\eta_I(y)-\left[1-\frac{\sigma}{2}\right]W_n(y+c_0t)-\frac{\sigma}{2}W_p(y-c_0t), \tag{24a}$$

$$D(y,t)=\eta_I(y)-\frac{\sigma}{2}W_n(y+c_0t)-\left[1-\frac{\sigma}{2}\right]W_p(y-c_0t). \tag{24b}$$

In (24)

$$\sigma(\gamma,\beta)=1-\left[\frac{\gamma(\cosh\beta-1)+\sinh\beta}{\gamma(\cosh\beta+1)+\sinh\beta}\right]^{1/2}, \tag{25}$$

where γ and β were defined in section 3. The ratio γ is >1 for canyons. The canyon number $\sigma\in\{0,1\}$ (for $\beta\in\{0,\infty\}$) is determined by the geometry of the system and is an important parameter in describing the geostrophic circulation of a canyon-shelf system. The wider the canyon is (hence the weaker the effects of one canyon edge on the circulation at the other edge), the smaller the canyon number is. It represents the interactive strength of one edge of the canyon on the circulation induced by the other edge.

The quantities $W_n(y+c_0t)$ and $W_p(y-c_0t)$ in (24) represent the information, which is the surface elevation in this case, transmitted into the study region by the long canyon waves from the positive y direction and negative y direction, respectively. The canyon wave that is induced by and intensified on the canyon edge at $x=-L$ carries the information $W_p(y+c_0t)$ and travels from the positive end of the canyon into the study region, whereas the canyon wave that is induced by and intensified on the canyon edge at $x=L$ carries the information $W_n(y-c_0t)$ and travels from the negative end of the canyon into the study region. Together they determine the final geostrophic state. We will use the physical meanings of $W_p(y+c_0t)$ and $W_n(y-c_0t)$ to study the geostrophic circulation for all our canyon models.

If $f<0$, A will equal the right-hand side of (24b) and D will equal the right-hand side of (24a). Therefore flow patterns in the southern hemisphere are the reverse of those in the northern hemisphere. The following discussion will be limited to the northern hemisphere ($f>0$).

Substituting (24) into (22a) and (22c), B and C can be found. Then substituting A, B, C, and D into (19) gives a solution of (1) expressed in terms of $W_p(y+c_0t)$ and $W_n(y-c_0t)$. As will be demonstrated in an example in the next subsection, this solution is the far-field geostrophic solution.

4.2. Far-field Solution for an Initial Surface Discontinuity

In the preceding discussion the initial conditions were quite general. To simplify further discussion, consider the simple, classical initial condition

$$\eta_I(y)=-\eta_0\,\mathrm{sgn}(y), \tag{26a}$$

$$u_I=v_I=0. \tag{26b}$$

For a flat-bottom open ocean with depth H_1, this initial condition will lead to a geostrophic state [*Gill*, 1982, pp. 191-203]

$$\eta(y)=-\eta_0\,\mathrm{sgn}(y)\left[1-\exp\left(-|y|/R_1\right)\right], \tag{27a}$$

$$u(y)=(gH_1)^{1/2}\frac{\eta_0}{H_1}\exp\left(-|y|/R_1\right), \tag{27b}$$

$$v=0, \tag{27c}$$

which represents a geostrophic jet with a width of $2R_1$ and a core at $y=0$.

Given a flat shelf (no shelf break), far away from the canyon ($|x|>>R_1+L$), the adjustment will be the same as that in a flat-bottom ocean, and the geostrophic state is described by (27). Far away from the core of this jet, initially, η is $-\eta_0$ for $y>>R_1$ and η_0 for $y<<-R_1$. This surface elevation information will have been transmitted along the canyon by the long canyon waves provided that $t>>1/|f|$. It is represented in (24) by $W_p(y+c_0t)$ and $W_n(y-c_0t)$. So for the specific initial condition (26), (24) reduces to (for $f>0$)

$$A(y,t)=\eta_0\begin{cases}-\sigma, & y>0,\\ (2-\sigma), & y<0,\end{cases} \tag{28a}$$

$$D(y,t)=\eta_0\begin{cases}-(2-\sigma), & y>0,\\ \sigma, & y<0.\end{cases} \tag{28b}$$

In the discussion above, (28) was obtained by considering the physical meaning of $W_p(y+c_0t)$ and $W_n(y-c_0t)$. However, (28) can also be obtained by using the purely mathematical method given below.

By using condition (20), (24) yields $W_n(z)=W_p(z)=\eta_I(z)$ where z is a free variable. So (24) can be written as

$$A(y,t)=\eta_I(y)-\left(1-\frac{\sigma}{2}\right)\eta_I(y+c_0t)-\frac{\sigma}{2}\eta_I(y-c_0t), \tag{29a}$$

$$D(y,t)=\eta_I(y)-\frac{\sigma}{2}\eta_I(y+c_0t)-\left(1-\frac{\sigma}{2}\right)\eta_I(y-c_0t). \tag{29b}$$

For the initial condition (26), in front of the wave front of the long wave ($|y|>c_0t$), (29) gives $A(y,t)=0$ and $D(y,t)=0$, so η remains $\eta_I(y)$ and $u=v=0$; i.e., the state has not been adjusted; behind the wave front of the long wave ($|y|<<c_0t$, which is equivalent to $t>>1/|f|$ because $|y|>>R_2>R_1=c_0/|f|$), (29) gives the same results as (28). The state has been adjusted by the long waves and

$$\eta(x,y,t)=-\eta_0\,\mathrm{sgn}(y)+\eta_0\left[\mathrm{sgn}(y)+(1-\sigma)\mathrm{sgn}(x)\right]\times\exp\left[(L-|x|)/R_1\right], \quad |x|>L, \tag{30a}$$

$$\eta(x,y,t)=-\eta_0\,\mathrm{sgn}(y)+\eta_0\left[\mathrm{sgn}(y)\frac{\cosh(x/R_2)}{\cosh(\beta/2)}+(1-\sigma)\frac{\sinh(x/R_2)}{\sinh(\beta/2)}\right], \quad |x|<L, \tag{30b}$$

$$u(x,y,t)=0, \tag{30c}$$

$$v(x,y,t)=-\left(\frac{g\eta_0}{fR_1}\right)\mathrm{sgn}(x)\left[\mathrm{sgn}(y)+(1-\sigma)\mathrm{sgn}(x)\right]\times\exp\left[(L-|x|)/R_1\right], \quad |x|>L, \tag{30d}$$

$$v(x,y,t)=\left(\frac{g\eta_0}{fR_1}\right)\frac{1}{\gamma}\left[\mathrm{sgn}(y)\frac{\sinh(x/R_2)}{\cosh(\beta/2)}+(1-\sigma)\frac{\cosh(x/R_2)}{\sinh(\beta/2)}\right], \quad |x|<L. \tag{30e}$$

Equations (30) describe a state that is independent of t and the value of y and that is valid only under the conditions $|y| >> R_2$ and $t >> 1/|f|$, i.e., it is the far field geostrophic solution. If t is finite, the transient effects due to shorter canyon waves will be present. It is obvious that the effects of the canyon on the geostrophic shelf circulation in the far-field decay exponentially with the distance from the nearer edge of the canyon. The width of the affected region is approximately R_1 on the shelf.

The solution (30), for two examples, is given outside the dashed lines in Figure 4. This figure shows the contours of surface elevation, which also form the streamlines. Details within the dashed lines, where the flow turns near the canyon edges, will be calculated in section 4.3. However, even for the far-field circulation, the picture that emerges is most intriguing. First, in the geostrophic state the canyon acts as a complete barrier to the approaching jet, which is completely deflected along the canyon. Second, as a jet approaches a canyon in the northern hemisphere, most of it is deflected to the right. Note also that the solution is symmetric about the origin. If the initial condition is changed so that the geostrophic flow direction is reversed, the flow pattern will be that of Figure 4 turned 180° around the z axis.

The canyon induces a flux along it that is of great interest. Integrating (27b) with respect to y for $y \in \{-\infty, \infty\}$ gives the flux approaching the canyon (in the $+x$ direction)

$$F_x = H_1 \int_{-\infty}^{\infty} u \, dy = \frac{2gH_1\eta_0}{f}. \tag{31}$$

Integrating (30d) and (30e) with respect to x for $x \in \{-\infty, \infty\}$ gives the net flux in the $+y$, along-canyon, direction

$$F_y = H_1 \int_{-\infty}^{-L} v \, dx + H_2 \int_{-L}^{L} v \, dx + H_1 \int_{L}^{\infty} v \, dx = F_x(\gamma^2 - 1)(1-\sigma). \tag{32}$$

If $f > 0$, then $F_x > 0$, and then $F_y > 0$. In the geostrophic state for a shelf-canyon system, the net flux transported in the along-canyon direction is proportional to the flux approaching the canyon and is to the left of the approaching flux; if γ is a constant, the wider the canyon (the smaller σ), the larger is F_y. The maximum transport is $F_x(\gamma^2 - 1)$ in the limit of infinitely wide canyon ($\beta \to \infty$ and hence $\sigma \to 0$).

4.3. Full Solution for an Initial Surface Discontinuity

In section 4.2 the analytic far-field solution was obtained. To complete the geostrophic solution of (4), we will use the far-field solution as the boundary conditions to calculate the solution in the regions where the streamlines turn, inside the dashed lines in Figure 4. In these regions, x and y are not very large compared with R_1 and R_2.

For the initial condition (26), the surface discontinuity (equation (2)) becomes

$$Q_I(x,y) = -\eta_I(y).$$

The solution of (4) should approach (30a) and (30b) as $|y| \to \infty$. Equations (30a) and (30b) give the far-field values of η at the two edges of the canyon as $-(1-\sigma)\eta_0$ at $x = -L$ and $(1-\sigma)\eta_0$ at $x = L$, respectively. As was stated in section 2, for a homogeneous, inviscid, linear fluid no flow can cross the edges of the canyon in the steady state, so η will be uniform along either edge of the canyon, i.e., $\eta_{-L} = -(1-\sigma)\eta_0$ at $x = -L$ and $\eta_L = (1-\sigma)\eta_0$ at $x = L$ for all values of y.

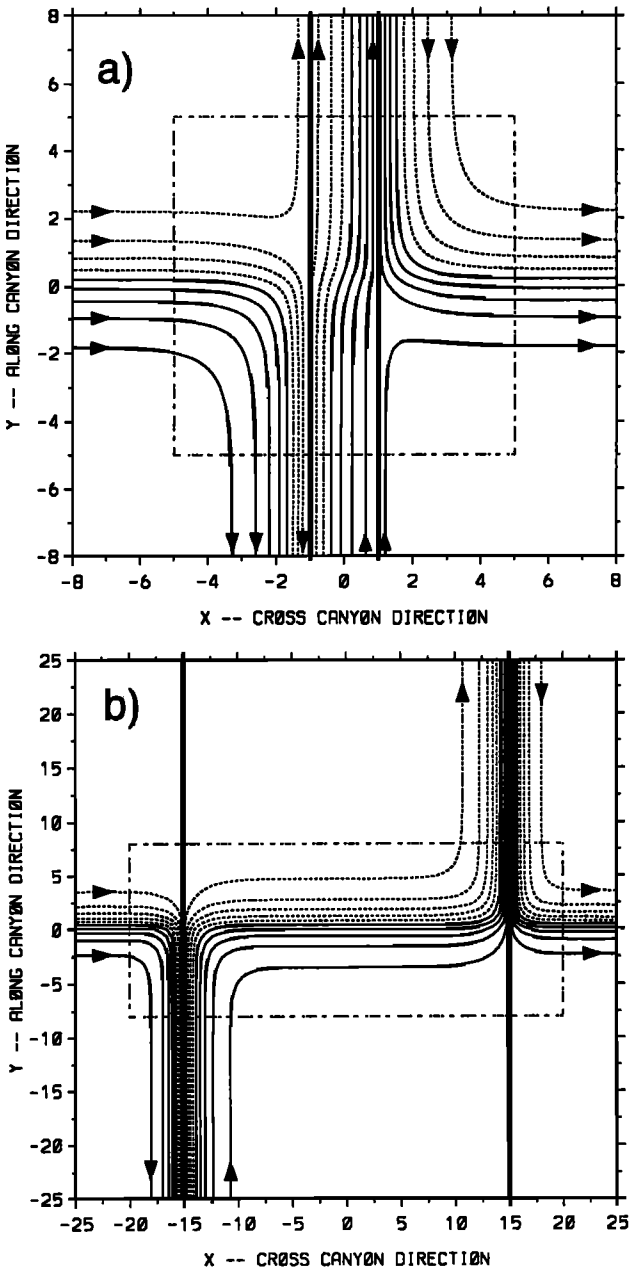

Figure 4. Contours of surface elevation η which also form the streamlines for the flat-bottom canyon. Thick lines represent the position of the canyon edges. Dotted lines represent negative η values. Arrows represent the direction of the flow in the northern hemisphere. The far-field solution applies outside the dashed lines. The range of values contoured is $-\eta_0$ to η_0, and the contour interval is $0.2\,\eta_0$. The position of the initial surface discontinuity is at y=0. The length unit is R_2, $\gamma^2 = 2$ and $\beta =$ (a) 2 and (b) 30.

The partial differential equation (4) will be solved first inside and then outside the canyon but only in the region $x < -L$ (from which the solution in the region $x > L$ can be easily derived owing to the symmetry of the solution).

Writing the solution of (4) as $\eta_2(x,y)$ inside the canyon and nondimensionalizing (4) with $(\tilde{x},\tilde{y}) = (x/R_2, y/R_2)$ and $\tilde{\eta}_2 = \eta_2/\eta_0$ gives

$$\frac{\partial^2 \tilde{\eta}_2(\tilde{x},\tilde{y})}{\partial \tilde{x}^2} + \frac{\partial^2 \tilde{\eta}_2(\tilde{x},\tilde{y})}{\partial \tilde{y}^2} - \tilde{\eta}_2(\tilde{x},\tilde{y}) = -\frac{\eta_I(\tilde{y})}{\eta_0}, \quad |\tilde{x}| < \frac{\beta}{2}. \tag{33a}$$

The boundary conditions are

$$\tilde{\eta}_2(\tilde{x}\to\pm\frac{\beta}{2},\tilde{y})=\pm(1-\sigma), \tag{33b}$$

$$\tilde{\eta}_2(\tilde{x},\tilde{y}\to\pm\infty)=\pm\left(\frac{\cosh\tilde{x}}{\cosh(\beta/2)}-1\right)+(1-\sigma)\frac{\sinh\tilde{x}}{\sinh(\beta/2)}. \tag{33c}$$

It is easy to demonstrate that a particular solution of (33a) is

$$\overline{\eta}(\tilde{y})=-\mathrm{sgn}(\tilde{y})\left[1-\exp\left(-|\tilde{y}|\right)\right]. \tag{34}$$

Applying the technique used by *Gill et al.* [1986], we put

$$\tilde{\eta}_2(\tilde{x},\tilde{y})=\overline{\eta}(\tilde{y})+\Phi_2(\tilde{x},\tilde{y}) \tag{35}$$

into (33). Using Fourier transforms and expressed in convolution form the solution is

$$\tilde{\eta}_2(\tilde{x},\tilde{y})=\overline{\eta}(\tilde{y})+(1-\sigma)\frac{\sinh\tilde{x}}{\sinh(\beta/2)}+(2\pi)^{-1/2}\int_{-\infty}^{\infty}E_2(\tilde{y}-\xi)G_2(\tilde{x},\xi)d\xi,\quad |\tilde{x}|<\frac{\beta}{2}, \tag{36}$$

where

$$E_2(\tilde{y}-\xi)=\mathrm{sgn}(\tilde{y}-\xi)\left[1-\exp\left(-|\tilde{y}-\xi|\right)\right],$$

$$G_2(\tilde{x},\xi)=\left(\frac{2}{\pi}\right)^{1/2}\int_0^{\infty}\frac{\cosh\left(\tilde{x}\left(p^2+1\right)^{1/2}\right)}{\cosh\left(\frac{\beta}{2}\left(\left(p^2+1\right)^{1/2}\right)\right)}\cos(\xi p)\,dp.$$

The typical shapes of $G_2(\tilde{x},\xi)$ versus ξ (for the examples of $\tilde{x}=0.2$, $\beta=2$ and $\tilde{x}=0.5$, $\beta=2$) and $E_2(y-\xi)$ versus ξ (for the examples of $\tilde{y}=0.5$ and $\tilde{y}=-1$) are shown in Figure 5, from which we see that $G_2(\tilde{x},\xi)$ decreases very quickly as $|\xi|$ increases. So (36) can be easily evaluated numerically (it is sufficient to take $|\xi|<10$ in the numerical evaluation).

Following the same procedure but writing the solution of (4) as $\eta_1(x,y)$ in the region $x<-L$ and changing to nondimensional variables $(\tilde{x},\tilde{y})=\left((x+L)/R_1, y/R_1\right)$ and $\tilde{\eta}_1=\eta_1/\eta_0$, (4) becomes

$$\frac{\partial^2\tilde{\eta}_1(\tilde{x},\tilde{y})}{\partial\tilde{x}^2}+\frac{\partial^2\tilde{\eta}_1(\tilde{x},\tilde{y})}{\partial\tilde{y}^2}-\tilde{\eta}_1(\tilde{x},\tilde{y})=-\frac{\eta_I(\tilde{y})}{\eta_0},\quad \tilde{x}<0. \tag{37a}$$

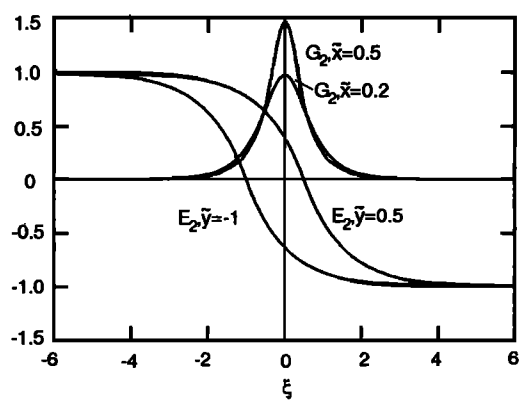

Figure 5. Shapes of $G_2(\tilde{x},\xi)$ (for $\tilde{x}=0.2$, $\beta=2$, and $\tilde{x}=0.5$, $\beta=2$) and $E_1(\tilde{y}-\xi)$ (for $\tilde{y}=-1$ and 0.5) versus ξ.

The boundary conditions are

$$\tilde{\eta}_1(\tilde{x}\to 0,\tilde{y})=-(1-\sigma), \tag{37b}$$

$$\tilde{\eta}_1(\tilde{x}\to-\infty,\tilde{y})=\overline{\eta}(\tilde{y}), \tag{37c}$$

$$\tilde{\eta}_1(\tilde{x},\tilde{y}\to\infty)=-1+\sigma\exp(\tilde{x}), \tag{37d}$$

$$\tilde{\eta}_1(\tilde{x},\tilde{y}\to-\infty)=1-(2-\sigma)\exp(\tilde{x}), \tag{37e}$$

where $\overline{\eta}(\tilde{y})$ is given by (34).

The solution of (37) is

$$\tilde{\eta}_1(\tilde{x},\tilde{y})=\overline{\eta}(\tilde{y})+\sigma\exp(\tilde{x})-\exp(\tilde{x})+(2\pi)^{-1/2}\int_{-\infty}^{\infty}E_1(\tilde{y}-\xi)G_1(\tilde{x},\xi)d\xi,\quad \tilde{x}<0, \tag{38}$$

where

$$E_1(\tilde{y}-\xi)=\mathrm{sgn}(\tilde{y}-\xi)\left[1-\exp\left(-|\tilde{y}-\xi|\right)\right],$$

$$G_1(\tilde{x},\xi)=(2\pi)^{-1/2}\int_{-\infty}^{\infty}\exp\left[\tilde{x}\left(p^2+1\right)^{1/2}\right]\exp(-i\xi p)dp$$

$$=-\left(\frac{2}{\pi}\right)^{1/2}\frac{\tilde{x}K_1\left[\left(\tilde{x}^2+\xi^2\right)^{1/2}\right]}{\left(\tilde{x}^2+\xi^2\right)^{1/2}},\quad \tilde{x}<0,$$

in which K_1 is the modified Bessel function as defined by *Abramowitz and Stegun* [1968].

The shapes of $G_1(\tilde{x},\xi)$ versus ξ and $E_1(\tilde{y}-\xi)$ versus ξ are quite similar to those of $G_2(\tilde{x},\xi)$ and $E_2(\tilde{y}-\xi)$, so (38) can also be rapidly evaluated numerically.

Combining (30a), and (30b), (36), and (38) gives the whole picture of the solution in the steady state as that shown in Figure 4. It can be seen that as the canyon becomes wider ($\beta\to\infty$), the flow pattern near either edge of the canyon is indistinguishable from that for a single-step topography derived by *Gill et al.* [1986]. This result is expected, since the effects of one edge of the canyon can not be felt at the other edge if the canyon becomes infinitely wide.

For Rossby adjustment over a flat-bottom canyon, the canyon acts as a complete barrier to the approaching geostrophic flow. The flow is diverted in both directions along the canyon, with most of the flow turning to the right in the northern hemisphere. Within the canyon, a unidirectional current is generated. A shelf-canyon system generates a net flux to the left of the shelf flow in the northern hemisphere, which decreases with increasing canyon number for a constant depth ratio of the system. The results mentioned above will be reversed in the southern hemisphere.

5. Geostrophic Solution Over a Stepped-Bottom Canyon

In the ocean the depth of a canyon is never uniform. As a first approximation to real situations, assume that the canyon is composed of two portions: a shallow upper canyon portion with constant depth H_2 and a deep lower portion with constant depth H_3 ($H_3>H_2$). If the length scale of the region where the depth changes from H_2 to H_3 is much shorter than the local Rossby radius, the bottom of the canyon can be represented by a step as shown in Figure 1. The canyon is assumed to be infinitely long with vertical walls, the step is at $y=d$, the width of the canyon is $2L$, and the depth of the shelf is H_1. The geostrophic solution around this stepped-bottom

canyon will be found by applying the results obtained in the preceding section. First, the far-field solution will be determined.

5.1. Analytical Far-Field Geostrophic Solution

Define the following parameters:

$$\gamma_i = (H_i / H_1)^{1/2},$$

$$\beta_1 = \frac{2L}{R_1},$$

$$\beta_i = \frac{\beta_1}{\gamma_i},$$

$$\sigma_i(\gamma_i,\beta_i) = 1 - \left[\frac{\gamma_i(\cosh\beta_i - 1) + \sinh\beta_i}{\gamma_i(\cosh\beta_i + 1) + \sinh\beta_i}\right]^{1/2}, \quad (39)$$

$$c_{0i} = c_1 \frac{|\gamma_i^2 - 1|}{(\gamma_i^2 + 2\gamma_i \coth\beta_i + 1)^{1/2}},$$

$$\varepsilon_i = (1-\sigma_i)(\gamma_i^2 - 1),$$

$$\varepsilon_{23} = (1-\sigma_2)(1-\sigma_3)(\gamma_3^2 - \gamma_2^2),$$

$$\delta_i = \frac{\varepsilon_i}{\varepsilon_2 + \varepsilon_3 + \varepsilon_{23}}, \quad (40)$$

where c_1 was given in section 3, and i=2, 3.

Assume that the region where $\partial\eta_I / \partial y \neq 0$ is a small, limited region around $y=0$. Far enough from the canyon bottom step and the region where $\partial\eta_I / \partial y \neq 0$, i.e., $|y| >> |d + R_2|$, the circulation will have the same pattern as that in the far field for a flat-bottom canyon. Thus the far-field solution for a stepped-bottom canyon can be expressed in the form of (23) in terms of the unknown η values at the canyon edges. In the geostrophic state, as was discussed in section 2, values of surface elevation η at the canyon edges and canyon bottom step must be constant so that there is no large-scale flow across the canyon edges or the canyon bottom step. Once these constants are found, the far-field geostrophic solution is given by (23).

The geostrophic state around a canyon is set up by canyon waves transmitting information in both directions along the canyon, as was discussed in the preceding section. Assume that the information (surface elevation η, in our case) transmitted in the -y and the +y directions is $W_{p2}(y+c_{02}t)$ and $W_{n2}(y-c_{02}t)$, respectively, in the region $y>d$, and $W_{p3}(y+c_{03}t)$ and $W_{n3}(y-c_{03}t)$, respectively, in the region $y<d$. The quantities $W_{n2}(y-c_{02}t)$ and $W_{p3}(y+c_{03}t)$ are the information carried away from the step, whereas $W_{p2}(y+c_{02}t)$ and $W_{n3}(y-c_{03}t)$ are the information carried from the positive and negative ends of the canyon toward the step. Write η at x=-L as η_{-L2} for $y>d$ and η_{-L3} for $y<d$, and η at x=L as η_L for $y<d$. The surface height at the step must be η_L because the double Kelvin wave propagating along the step will carry the information η_L away from the x=L edge. Similarly, η at x=L for $y>d$ is also η_L. Since η_L is generally not equal to η_{-L2} or η_{-L3}, there must be a singularity where the step meets the x=-L edge. Similar to the case discussed by *Gill et al.* [1986] in which double Kelvin waves propagate along a step toward a wall, there should be flux across the step (and in our case the x=-L edge), through the singular point, in order to conserve mass.

In the linear steady state the transport across a line between two points P and Q (say) in a region of depth H is

$$\frac{gH}{f}(\eta_P - \eta_Q),$$

to the right. Thus in our case, writing $\eta|_{x\to-\infty} = \eta^0_{-\infty}$ and $\eta|_{x\to\infty} = \eta^0_{\infty}$ at y=d, the flux across $y = d+\mu$, where μ is infinitesimal is

$$\frac{g}{f}\left[H_1(\eta_{-L2} - \eta^0_{-\infty}) + H_2(\eta_L - \eta_{-L2}) + H_1(\eta^0_{\infty} - \eta_L)\right],$$

and the flux across $y = d-\mu$ is

$$\frac{g}{f}\left[H_1(\eta_{-L3} - \eta^0_{-\infty}) + H_3(\eta_L - \eta_{-L3}) + H_1(\eta^0_{\infty} - \eta_L)\right].$$

The requirement that these two fluxes are equal at $y = d$ is

$$(\gamma_3^2 - \gamma_2^2)\eta_L + (\gamma_2^2 - 1)\eta_{-L2} - (\gamma_3^2 - 1)\eta_{-L3} = 0. \quad (41a)$$

In the regions far away from both the core of the geostrophic flow and the step, analogous to (24), for f>0

$$\eta_L = \frac{\sigma_2}{2} W_{p2}(y+c_{02}t) + (1-\frac{\sigma_2}{2}) W_{n2}(y-c_{02}t), \quad (41b)$$

$$\eta_{-L2} = (1-\frac{\sigma_2}{2}) W_{p2}(y+c_{02}t) + \frac{\sigma_2}{2} W_{n2}(y-c_{02}t), \quad (41c)$$

from consideration of the region $y<d$, and

$$\eta_L = \frac{\sigma_3}{2} W_{p3}(y+c_{03}t) + (1-\frac{\sigma_3}{2}) W_{n3}(y-c_{03}t), \quad (41d)$$

$$\eta_{-L3} = (1-\frac{\sigma_3}{2}) W_{p3}(y+c_{03}t) + \frac{\sigma_3}{2} W_{n3}(y-c_{03}t). \quad (41e)$$

from consideration of the region $y>d$.

Combining (41), the solution expressed in terms of $W_{p2}(y+c_{02}t)$ and $W_{n3}(y-c_{03}t)$ can be found:

$$\eta_L = \frac{\sigma_3}{2}(2\delta_2 W_{p2}) + (1-\frac{\sigma_2}{2})(2\delta_3 W_{n3}), \quad (42a)$$

$$\eta_{-L2} = (1-\frac{\sigma_2}{2}) W_{p2} + \frac{\sigma_2}{2}\left[(2\delta_3 W_{n3}) + (1-2\delta_3) W_{p2}\right], \quad (42b)$$

$$\eta_{-L3} = (1-\frac{\sigma_3}{2})\left[(2\delta_2 W_{p2}) + (1-2\delta_2) W_{n3}\right] + \frac{\sigma_3}{2} W_{n3}, \quad (42c)$$

where σ_i and δ_i (i = 2, 3) are given by (39) and (40), respectively. Equations (42) are the general geostrophic far-field solution around a stepped-bottom canyon for a nonspecific initial condition.

When $H_2 = H_3$ (so $\varepsilon_2 = \varepsilon_3$, $\varepsilon_{23} = 0$, and $\delta_2 = \delta_3 = 0.5$), η_{-L2} and η_{-L3} are identical. Together with η_L they are consistent with the results for a flat-bottom canyon.

If the initial condition is a surface discontinuity (equations (26)), similar to the last section, $W_{p2}(y+c_{02}t)$ and $W_{n3}(y-c_{03}t)$ in (42) are $-\eta_0$ and η_0, respectively. The corresponding solution is

$$\eta_L = \left[(2-\sigma_2)\delta_3 - \sigma_3\delta_2\right]\eta_0, \quad (43a)$$

$$\eta_{-L2} = \left[2\delta_3\sigma_2 - 1\right]\eta_0, \quad (43b)$$

$$\eta_{-L3} = \left[1 - 2\delta_2(2-\sigma_3)\right]\eta_0. \quad (43c)$$

Equations (42) or (43) with (23) give the far-field geostrophic solution for η around a stepped-bottom canyon.

The flux approaching a stepped-bottom canyon under the initial condition (26) is F_x given by (31), whereas the flux in the along-canyon direction is

$$F_y = 2\varepsilon_3\delta_2 F_x = 2\varepsilon_2\delta_3 F_x. \quad (44)$$

If $H_2 = H_3$, (44) is identical to (32), the value for the flat-bottom canyon. Again, there is a net flux generated in the along-canyon direction to the left of the approaching shelf flow in the northern hemisphere.

5.2. Numerical Full Geostrophic Solution

The geostrophic solution near the canyon edges and the step may be calculated from the far-field solution assuming geostrophy. However, as was discussed for a similar case by *Gill et al.* [1986], in practice, geostrophy will not occur everywhere for a stepped-bottom canyon as a result of nonlinear or frictional effects and the advection of potential vorticity through the singularity. The solution achieved by solving (4) can be regarded only as a first approximation.

The complicated geometry of a stepped-bottom canyon makes an analytic solution complicated. Consider instead a numerical solution of (4). After multiplying by the grid space size, the finite difference form of the elliptic type equation (4) is

$$\eta_{i+1,j} + \eta_{i-1,j} + \eta_{i,j+1} + \eta_{i,j-1} + e_{i,j}\eta_{i,j} = f_{i,j} \qquad (45)$$

where i/j is the grid index in x/y dimension of a square domain. The coefficients $e_{i,j}$ and $f_{i,j}$ can be calculated from the grid space and the canyon system parameters γ_2 and γ_3. If the domain is large enough, (27a) and (30a) and (30b) can be used as the domain boundary condition. In fact, the numerical solution of (45) is done in pieces with boundary conditions given by (43) along all depth discontinuities. The singularity also occurs on a boundary. With the Chebyshev acceleration and a reasonable tolerance, the solution of (45) is calculated by simultaneous overrelaxation [*Press et al.*, 1986, pp. 657-659]. The precision of the solution has been checked by comparing different spatial resolutions.

Solutions of (45) for some examples are given in Figure 6, which shows the contours of surface elevation, which also form streamlines. Because the Rossby radius over a stepped-bottom canyon has different values for the deep and shallow portions, the Rossby radius on the shelf, R_1, is chosen as the length scale instead of the Rossby radius over the canyon.

As is shown in the three panels of Figure 6, a stepped-bottom canyon is not a complete barrier to an approaching shelf flow. The shelf flow can cross the canyon edge in a small region where the junction occurs between the step in the canyon bottom and the left canyon edge (looking upcanyon) in the northern hemisphere; a stepped-bottom canyon can also induce an along-canyon flux that is directed to the left of the approaching shelf flow in the northern hemisphere. Note that the solution is no longer symmetric owing to the existence of the step. Figures 6a and 6b, compared with Figure 4a, show

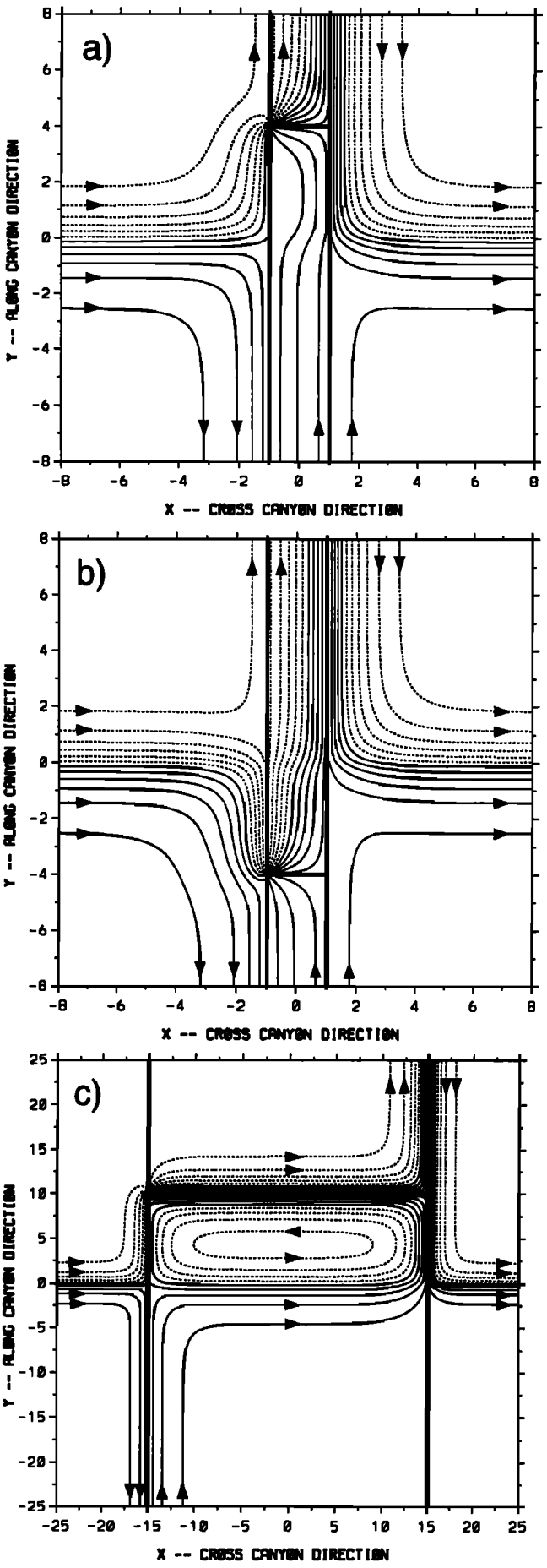

Figure 6. Contours of surface elevation η, which also form the streamlines, for the stepped-bottom canyon. Thick lines represent the position of the canyon edges and the canyon bottom step. Dotted lines represent negative η values. Arrows represent the direction of the flow in the northern hemisphere. The range of values contoured is $-\eta_0$ to η_0. The position of the initial surface discontinuity is at y=0. The length unit is R_1, $\gamma_2^2 = 2$, $\gamma_3^2 = 4$, (a) The step is at y=4, $\beta_1 = 2$, the grid points are 385 x 385, and the contour interval is $0.16\,\eta_0$. (b) The step is at y=-4, $\beta_1 = 2$, the grid points are 385 x 385, and the contour interval is $0.16\,\eta_0$. (c) The step is at y=10, $\beta_1 = 30$, the grid points are 401 x 401, and the contour interval is $0.2\,\eta_0$.

that the flow on the right-hand side of the canyon (looking up-canyon) is almost unaffected by the slope; however, on the left-hand side, much of the approaching flow that for a flat-bottom canyon would turn right, is deflected into the canyon. In Figure 6c the canyon is wide enough that the two sides are essentially decoupled. The solution in the canyon in the region of the junction between the step and the canyon edge is similar to that observed by *Gill et al.* [1986] for a channel but modified by the source of fluid from the shelf.

6. Geostrophic Circulation Over a Sloping-Bottom Canyon With a Coast and a Shelf Break

6.1. Values of the Surface Elevation at Depth Changes

This geometry (shown in Figure 2) has the gross features of Juan de Fuca Canyon including the shelf break, the coastline broken by the Strait of Juan de Fuca and variations of bottom depth. For convenience, the initial condition (26) is chosen with the fluid at rest and with a surface discontinuity along a line in the across-canyon direction.

It is assumed that the coast is at $y = d_c$, the shelf break is at $y = d_{SB}$, the lower bound of the canyon head slope is at $y = d_{hl}$ while the upper bound of the slope is at $y = d_{hu}$, and the lower bound of the canyon mouth slope is at $y = d_{ml}$ while the upper bound of the slope is at $y = d_{mu}$.

The depth ratios in this model are defined as

$$\gamma_j = R_j / R_1 = \left(h_j / h_1\right)^{1/2}, \quad j = 0,2,3, \tag{46}$$

where R_j is the barotropic Rossby radius corresponding to depth h_j. Specifically, h_0 is the depth of the strait, h_1 is the depth on the shelf, h_2 is the depth of the middle canyon portion, and h_3 is the depth of the deep canyon portion and the deep ocean.

To solve for the case with a canyon, the surface elevation at the coast and shelf break in the case without a canyon are required. This solution can be found by assuming geostrophy, no variation in the along-shelf direction, and conservation of potential vorticity. Boundary conditions include no flow through the coast, mass flux conservation over the shelf break and conservation of mass. A full derivation is given by *Chen* [1996, Appendix C]. The required surface elevation values are as follows: At the shelf break,

$$\eta_{LC} = \eta_0\left[A\exp(D_{SB3}) + 1\right] \tag{47a}$$

and at the coast

$$\eta_k = \eta_0\left[2E\exp(D_c) - 1\right] \tag{47b}$$

where

$$A = \left\{2\left[1 - \exp(2D_c)\right]\right\}\left\{\exp(D_{SB3} - D_{SB1})\right.$$
$$\left.\times\left[(\gamma_3 - 1)\exp(2D_{SB1}) + (\gamma_3 + 1)\exp(2D_c)\right]\right\}^{-1},$$
$$E = \left\{2\exp(D_{SB3})\left[\gamma_3\cosh(D_{SB1}) - \sinh(D_{SB1})\right]\right\}$$
$$\times\left\{2\exp(D_{SB3})\left[\gamma_3\cosh(D_{SB1}) - \sinh(D_{SB1})\right]\right.$$
$$\left.\times\left[(\gamma_3 - 1)\exp(2D_{SB1}) + (\gamma_3 + 1)\exp(2D_c)\right]\right\}^{-1}$$

and $D_{SB1} = d_{SB} / R_1$, $D_{SB3} = d_{SB} / R_3$, and $D_c = d_c / R_1$.

Now consider the case with a canyon as shown in Figure 7. At the coast and at all changes in depth, the surface height will be a constant as discussed in section 2. The waves, Kelvin waves induced by the coast and double Kelvin waves induced by the shelf break, are one sided; they propagate with the shallower water or the coast on the right. Following the direction of propagation of these waves and of the double Kelvin waves over the canyon slopes allows calculation of the surface height at all the depth changes.

Because Kelvin and double Kelvin waves can propagate only in the $-x$ direction, the existence of the canyon and the strait does not affect the adjustment process for $x \to \infty$. Thus in the steady state, the surface elevation at the coast (denoted η_K) is given by (47b), and the surface elevation at the shelf break (denoted η_{LC}) is given by (47a).

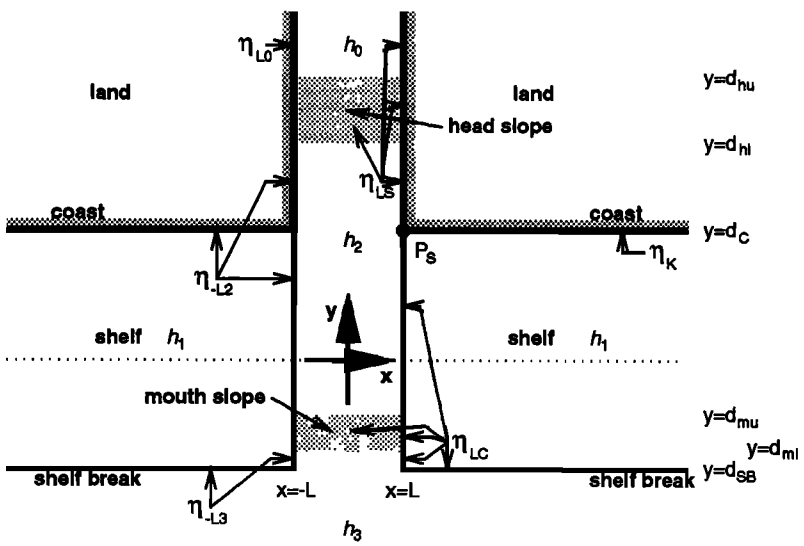

Figure 7. Top view of the Juan de Fuca model canyon. The shaded regions represent the canyon bottom slopes. The dotted line represents the position of the initial surface discontinuity. The width of the canyon as well as the strait is $2L$. The depths in the inner strait, on the shelf over the middle canyon, and over the deep canyon (as well as in the deep ocean) are h_0, h_1, h_2 and h_3, respectively. The surface elevation in the geostrophic state at all depth changes and boundaries is indicated. See text for other notations.

At the part of the canyon edge at $x = L$ between the shelf break and the canyon mouth slope, which is contiguous with the shelf break, the surface elevation must be the same value as that at the shelf break for $x > L$, η_{LC}.

The surface elevation at the canyon edge at $x = L$ is transmitted by the canyon waves along the canyon edge in the $+y$ direction and transmitted by the slope-induced topographic waves towards the canyon edge at $x = -L$. Regardless of the shape of the slope, the surface elevation over it is a constant, η_{LC}, determined by the canyon waves. A constant surface elevation over the slope implies that the fluid there, in the geostrophic state, is stagnant (see *Allen* [1996a] for details). The canyon waves carry the surface height η_{LC} to the edge of the strait.

Beyond the canyon head slope, in the geostrophic state, the surface elevation is uniform along the strait walls. If the surface elevation along the strait wall at $x = L$ in the lower strait is assumed to be η_{LS}, the Kelvin waves within the strait will transmit this information along the strait wall at $x = L$ toward the $+y$ direction. Similar to the analysis for the canyon mouth slope, the canyon head slope does not interfere with the transmission of the information along the strait wall at $x = L$. The information η_{LS} will be transmitted continuously along the whole length of the strait wall at $x = L$ and transmitted by the slope-induced topographic waves toward the strait wall at $x = -L$.

Note that η_{LS} is equal to neither η_{LC} nor η_K. Thus P_S is a singular point similar to that discussed in section 5. At P_S, where the coast meets the canyon edge at $x = L$, the incoming Kelvin waves which carry the information η_K confront the incoming canyon waves which carry the information η_{LC}. The outgoing Kelvin waves from P_S propagate along the strait wall at $x = L$ and transmit the information η_{LS} in the $+y$ direction.

Along the strait wall at $x = -L$, the Kelvin waves that propagate in the $-y$ direction toward the head slope make the surface elevation a constant denoted η_{-LO}. However, in the region where the strait wall at $x = -L$ meets the canyon head slope, these incoming Kelvin waves confront the incoming slope-induced topographic waves that carry the information η_{LS}. The outgoing Kelvin waves that propagate toward the mouth of the strait make the surface elevation along the strait wall at $x = -L$ in the lower strait a constant denoted η_{-L2}. The region where the canyon head slope meets the strait wall at $x = -L$ is a singular line, an extension of the singular point discussed in section 5.

When the Kelvin waves reach the junction of the coast and the canyon edge at $x = -L$, the task of transmitting the information, η_{-L2}, is handed over to Kelvin waves that propagate in the $-x$ direction along the coast and the canyon waves that propagate toward the canyon mouth slope.

The region where the canyon edge at $x = -L$ meets the canyon mouth slope is another singular line. The outgoing canyon waves that propagate away from this region make the surface elevation along the canyon edge at $x = -L$ in the deep canyon portion a constant denoted η_{-L3}.

The double Kelvin waves that propagate in the $-x$ direction along the shelf break for $x < -L$ make the surface elevation at the shelf break η_{-L3}.

The geostrophic solution of the steady state governing equation (4) at all depth changes and boundaries has been analyzed qualitatively and is indicated in Figure 7 for easy reference. Now the relations between these surface elevations must be found using conservation of mass and the properties of Kelvin waves.

Solution for η_{LS}. Equating the flux across the lines $y = d_c - \varepsilon$, $x \in \{-X, X\}$, and $y = d_c + \varepsilon$, $x \in \{-L, L\}$, where $\varepsilon \to 0$ and $X \to \infty$ shown in Figure 8a, gives

$$\eta_{LS} = \frac{(\gamma_2^2 - 1)\eta_{LC} + \eta_k}{\gamma_2^2}. \tag{48}$$

Solution for η_{-LO}. A strait acts similarly to a canyon with the canyon waves replaced by Kelvin waves. Thus the surface elevation at the two walls of the inner strait beyond the canyon head slope is given by

$$\eta_{LS} = \frac{\sigma_s}{2} W_{ns}(y + c_{os}t) + \left(1 - \frac{\sigma_s}{2}\right) W_{ps}(y - c_{os}t), \tag{49a}$$

$$\eta_{-L0} = \left(1 - \frac{\sigma_s}{2}\right) W_{ns}(y + c_{os}t) + \frac{\sigma_s}{2} W_{ps}(y - c_{os}t), \tag{49b}$$

where $W_{ns}(y + c_{os}t)$ is the information carried by the Kelvin waves from the farthest end of the strait toward the canyon head slope, $W_{ps}(y - c_{os}t)$ is the information carried by the Kelvin waves moving in the $+y$ direction, and $\sigma_s = 1 - \tanh(\beta/2)$.

Eliminating $W_{ps}(y - c_{os}t)$ between (49a) and (49b) gives

$$\eta_{-L0} = \frac{\sigma_s \eta_{LS} + 2(1 - \sigma_s) W_{ns}}{2 - \sigma_s} \tag{50}$$

where $W_{ns} = -\eta_0$ for the chosen initial condition (26).

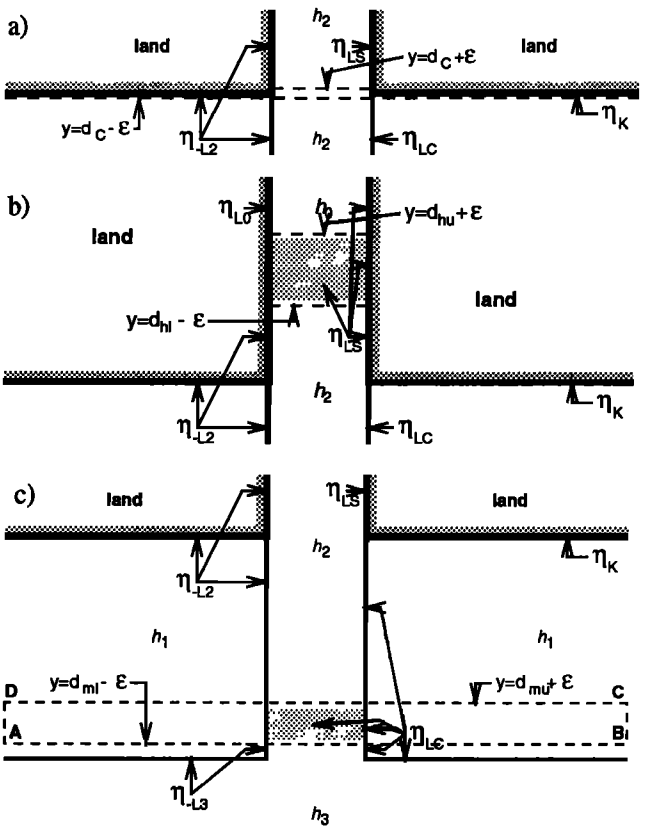

Figure 8. Close up views of the Juan de Fuca model canyon near (a) the mouth of the strait, (b) the canyon head slope, and (c) the canyon mouth slope. The surface elevation in the geostrophic state at all depth changes is indicated.

Solution for η_{-L2}. Equating the flux across the lines $y = d_{hl} - \varepsilon$ and $y = d_{hu} + \varepsilon$, where $\varepsilon \to 0$ and $x \in \{-L, L\}$ shown in Figure 8b, gives

$$\eta_{-L2} = \frac{\left(\gamma_2^2 - \gamma_0^2\right)\eta_{LS} + \gamma_0^2 \eta_{-L0}}{\gamma_2^2}, \tag{51}$$

where γ is defined by (46).

Solution for η_{-L3}. Consider the rectangle shown in Figure 8c, which includes the canyon mouth slope. The four points of the rectangle are $A(-X, d_{ml} - \varepsilon)$, $B(X, d_{ml} - \varepsilon)$, $C(X, d_{mu} + \varepsilon)$, and $D(-X, d_{mu} + \varepsilon)$, in which $\varepsilon \to 0$ and $X \to \infty$. Forcing the mass flux entering the box to be zero for the steady geostrophic state gives

$$\eta_{-L3} = \frac{\left(\gamma_3^2 - \gamma_2^2\right)\eta_{LC} + \left(\gamma_2^2 - 1\right)\eta_{-L2}}{\left(\gamma_3^2 - 1\right)}. \tag{52}$$

Solutions of the steady state governing equation (4) have been obtained at all depth changes (the canyon bottom slopes, the canyon edges, and the shelf break) and at all internal boundaries (the coast and the strait walls). Equation (4) can now be solved in each flat-bottom segment following the numerical procedure discussed in section 5.2.

6.2 Numerical Solution for Full Domain

The steady state governing equation (4) was integrated in a square domain several Rossby radii in width. The values of the surface height at all the depth changes were taken from the results of the previous section. The solutions at the open boundaries are as follows.

1. The solution at the right (southern) boundary is the geostrophic solution over a single step parallel to a coast without a canyon as discussed in the preceding section. The full solution is given by *Chen* [1996].
2. The solution at the left (northern) boundary is the geostrophic solution over a single step parallel to a coast forced to have surface elevations at the coast and shelf break given by η_{-L2} and η_{-L3}, respectively. The full solution is given by *Chen* [1996].
3. The solution at the bottom (deep ocean) boundary is estimated from the surface elevation at the right and left bottom corners by linear interpolation.
4. The solution at the top (strait) boundary is given by the solution for geostrophic flow constrained by the values of the surface elevation at the strait walls, η_{-L0} and η_{LS}.

The results of the numerical integration for two sizes of canyon are given. First consider a canyon with width of 1 Rossby radius (the barotropic Rossby radius on the shelf) and length of 4 Rossby radii. The depths are 100 m in the inner strait, 150 m on the shelf, 300 m in the middle canyon and 1800 m in the deep canyon and over the deep ocean. Relative to the line of the surface discontinuity (at $y = 0$), the coast is at 3 Rossby radii, the shelf break is at -1 Rossby radius, and the two canyon slopes are located between 3.75 and 4.5 and between -0.6 and 0.2, again in Rossby radii. The distribution of the surface elevation is shown in Figure 9a, and a close-up of the flow vectors in the region of the canyon is given in Figure 9b.

Similar to the stepped-bottom canyon, this geometry is not a complete barrier to the incoming shelf break current, part of which crosses the canyon walls at the canyon mouth slope. Some flow is diverted from outside the shelf break into the canyon through the mouth. Some of the flow in the canyon "squeezes" out of the canyon through the singular point where the coast meets the right canyon edge.

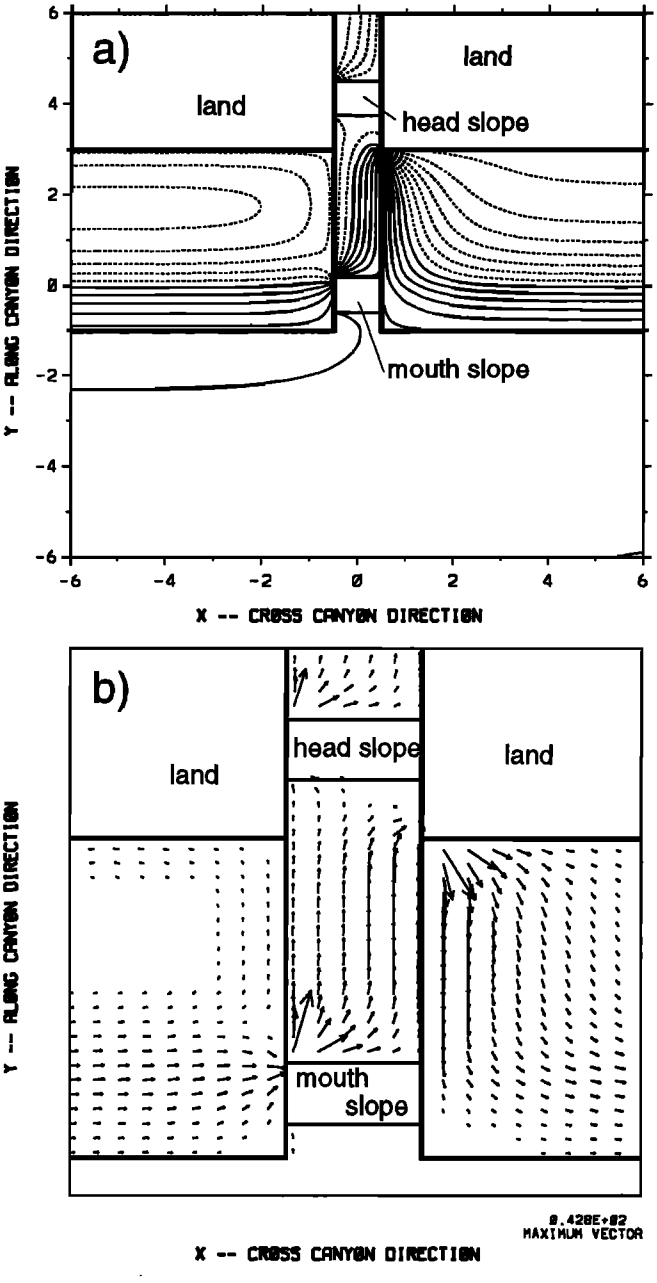

Figure 9. Geostrophic state around the large size Juan de Fuca model canyon. (a) Contours of the surface elevation η. (b) Velocity field around the canyon; note that this is an expanded view. The thick lines represent the positions of the canyon edges, shelf break, coast, strait walls and boundaries of the canyon bottom slopes. Solid lines in Figure 9a represent positive η, while dotted lines represent negative η. The length scale is R_1. The range of η contoured is from $-\eta_0$ to η_0, and the contour interval is 0.14 η_0 where η_0 is half the height of the initial surface discontinuity, which was taken as 0.2 m in this example.

The second canyon size chosen corresponds to the geometry of Juan de Fuca Canyon. The depths are the same as in the previous case, but the canyon is 14 km wide (0.04 Rossby radii) and the shelf is 70 km wide (0.2 Rossby radii). The cal-

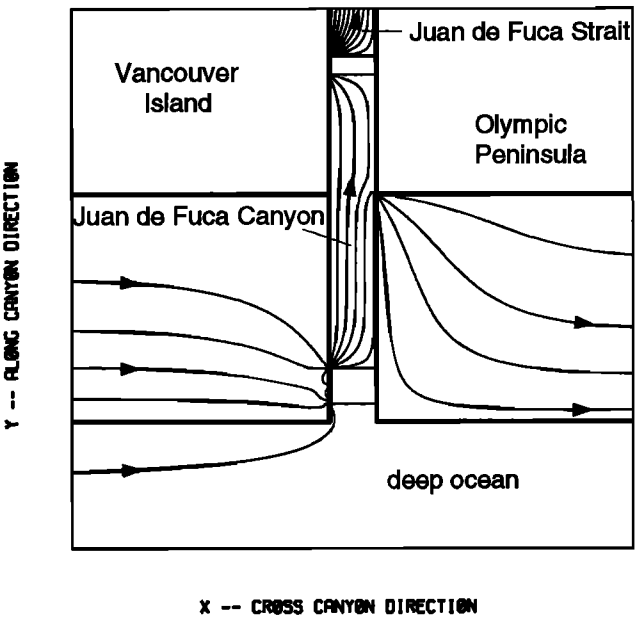

Figure 10. Geostrophic state around the model of Juan de Fuca canyon. Only the inner grid is shown. The thin lines are contours of the surface elevation η, which are also the streamlines in the geostrophic state. Thick lines represent the positions of the canyon edges, shelf break, coast, strait walls, and boundaries of the canyon bottom slopes. Arrows represent the direction of flow during a southerly coastal flow. The range of η contoured is from 0.5 η_0 to 0.98 η_0, and the contour interval is 0.01 η_0, where η_0 is half the height of the initial surface discontinuity.

culation was done using a nested grid method. The first relaxation was done for a 6 Rossby radii by 6 Rossby radii domain. Then, relaxation was done on a smaller grid (shown in Figure 10) using, as open boundary conditions, values interpolated from the original large grid. Contours of surface height, which are the streamlines are shown in Figure 10.

In the region of Juan de Fuca Canyon, the observed circulation is determined by a competition among several different physical processes including estuary effects, wind, and topographic effects. However, even with neglect of stratification, some features of the flow around Juan de Fuca Canyon are simulated by this simple model. First, as was predicted by previous models and in agreement with this model, the southbound shelf break current leads to an in-canyon flow as observed by *Freeland and Denman* [1982]. Second, at the mouth of Juan de Fuca Strait, the flow around the corner of the Olympic Peninsula is strong and multidirectional [*Thomson et al.*, 1989]. Third, the model predicts cyclonic flow to the north of the canyon (most clearly seen in Figure 9a) in the region where the Tully eddy is observed. The model does not give a closed eddy, which is to be expected; the presence of nonlinearity and the surface outflow from Juan de Fuca Strait must play a role. Fourth, the model shows a shift of the position of the shelf break current as it flows over the canyon to further inshore. Unfortunately, there are no detailed observations of the shelf current off the Olympic Peninsula to confirm or refute this prediction.

Some other properties of flow around this geometry include the following.

1. Unlike the infinitely long canyons, the streamlines are not symmetric owing to the existence of the shelf break. If the initial condition is changed so that the geostrophic flow direction is reversed, the flow patterns will be similar to those shown except with all flow directions reversed.

2. A canyon can cause the inshore excursion of a shelf break current of either direction, but the net transport along the canyon and the flow within the canyon is always to the left of the shelf break current in the northern hemisphere.

7. Discussion

The analysis in this paper is based on the linear shallow water equations for the barotropic case and thus represents the strongest effects of the topography on the flow. Once stratification is considered, our results should be modified (see *Allen* [1996b] for the narrow canyon case). The barotropic solution can be directly extended to a special baroclinic case. If reduced gravity is used and hence the deformation scale is the internal Rossby radius, all results in this paper are retained in the bottom layer of a system with a relatively deep overlying layer (one and a half layer stratified model [*Gill et al.*, 1986]).

In this paper, the dispersion relation for canyon waves has been calculated. The properties of long canyon waves are discussed and are essential for determining the geostrophic state. The wave solution is not given in this paper, and thus the adjustment problem posed in section 2 is only partially solved. Even so, some basic properties of the effect of canyons on shelf circulation have been revealed. Some important parameters defined in the process are σ and c_0, and they are expected also to be significant for the wave solution.

The canyon number σ is an important parameter for describing the geostrophic state around a canyon. The value of σ is determined by the geometry of the canyon system, i.e., the depth of the water layer on the shelf and over the canyon, the width of the canyon, and the Rossby radius over the canyon. For the bottom layer of the special baroclinic model, the one and half layer model, three canyons (Juan de Fuca Canyon, Astoria Canyon, and Moresby Trough) are chosen to illustrate the values of σ for real canyon systems (however, note that the upper layer is not relatively deep compared with the bottom layer, so the calculations give only the approximate values of σ). For the Juan de Fuca Canyon system the depth of the bottom layer is assumed to be 50 m on the shelf and 250 m over the canyon; the average width of the canyon is 7 km, while the local internal Rossby radius is about 20 km [*Freeland and Denman*, 1982]. Thus the calculated σ is 0.684. For Astoria Canyon the depth of the bottom layer is assumed to be 50 m on the shelf and 500 m over the canyon; the average width of the canyon is 7 km, while the local internal Rossby radius is about 30 km (B.M. Hickey, The response of a narrow canyon to strong wind forcing, submitted to *Journal of Physical Oceanography* 1996, hereinafter referred to as B.M. Hickey, submitted manuscript, 1996). Thus the calculated σ is 0.880. For Moresby Trough the depth of the bottom layer is assumed to be 50 m on the shelf and 250 m over the canyon; the average width of the canyon is 40 km, while the local internal Rossby radius is about 20 km [*Crawford et al.*, 1985]. Thus the calculated σ is 0.171. Thus Astoria canyon is narrow with strong coupling between the two sides, Moresby Trough is wide with weak coupling, and Juan de Fuca lies in between.

A simple classical initial condition was used in most of the discussion. As long as the forcing is small enough that the flow remains approximately linear, solutions for other initial conditions can be found by linear superposition.

The topography involved is simplified but contains the basic features of a real canyon. Studying the circulation around a flat-bottom canyon lays the foundations for analyzing that around a more realistic, complicated canyon. The circulation pattern for an infinitely wide flat-bottom canyon is identical to that derived by *Gill et al.* [1986] for a single-step topography, which has been demonstrated to be consistent with numerical and laboratory experiments [*Gill et al.*, 1986]. To study a canyon with a stepped bottom is the first step toward studying a real, sloping-bottom canyon. Then a geometry was chosen that has the major features of Juan de Fuca Canyon, including the shelf break, coast, and Strait of Juan de Fuca.

Extension of the results of this paper must be made carefully on account of the linear and inviscid assumptions. For instance, our results for a very narrow, infinitely long flat-bottom canyon will lead to currents within the canyon too strong to have physical meaning. This deficiency is probably due to neglecting the effects of turbulent viscosity or advection. Inclusion of viscosity and nonlinear advection in a stratified fluid is expected to improve our current theory.

Our theoretical results are qualitatively consistent with some observations. For example, the mean shelf break current along the west coast of Vancouver Island, where the Juan de Fuca Canyon is located, is southeastward in the summer. A mean in-canyon current within the Juan de Fuca Canyon was observed in the summer [*Freeland and Denman*, 1982]. When a northwestward shelf break current is forced by a winter storm in this region, an out-canyon current within the canyon was observed [*Cannon*, 1972]. However, the current magnitudes predicted here, approximately equal in the canyon to that over the shelf, are a factor of 3 too high compared with *Cannon*'s [1972] observations. The overprediction is expected; the approximation of homongeneous flow tends to overestimate the effect of the topography.

The theoretical results are also verified by the observations around the Hudson Shelf Valley [*Mayer et al.*, 1982], where the strongest in-canyon and out-canyon flows are associated with northeastward and southwestward winds (and hence shelf currents), respectively. All these observations are consistent with the prediction from our model with a shelf break. Using the conductivity-temperature-depth data from specific La Perouse cruises, *Foreman* [1992] simulated the summer geostrophic current in the coastal area southwest of Vancouver Island with a numerical model. The model results show that upwelling is associated with horizontal velocity excursions of the shelf break current onto the shelf through the canyons in this region. The dynamics for the horizontal movement of the currents around the canyons have not been given. Our theoretical analysis provides a possible explanation of Foreman's numerical results. The shelf break current has also been observed to turn shoreward and have a strong velocity component upcanyon over Astoria Canyon during periods of weakly vertically sheared southerly flow (B.M. Hickey, submitted manuscript, 1996).

8. Conclusions

In this paper the geostrophic adjustment method has been used to study the influence of submarine canyons on geostrophic shelf currents. The fluid is homogeneous, inviscid, and on an f plane. Some conclusions can be drawn.

1. The subinertial, double Kelvin waves over a canyon determine the geostrophic solution. These waves can propagate in either direction along the canyon but are trapped to one of the canyon edges along which they propagate, keeping the deep water of the canyon to their left in the northern hemisphere. All but very long canyon waves are dispersive.

2. An important parameter for describing the geostrophic state around a canyon is the canyon number σ, which is determined by the geometry of the canyon system ($\sigma \in \{0,1\}$), for an infinitely narrow canyon $\sigma \to 1$ and for an infinitely wide canyon $\sigma \to 0$. The canyon number measures the influence of one canyon edge on the other.

3. For an infinitely long flat-bottom canyon, the canyon acts as a complete barrier to an approaching shelf flow in the geostrophic state. The net transport along the canyon is to the left of the approaching geostrophic flow in the northern hemisphere.

4. For an infinitely long stepped-bottom canyon the canyon is not a complete barrier to an approaching shelf flow in the geostrophic state. In the northern hemisphere, flow crosses at the singular point where the left canyon edge (looking upcanyon) meets the canyon bottom step. The net transport along the canyon is to the left of the approaching geostrophic flow in the northern hemisphere.

5. For a canyon with geometry similar to Juan de Fuca, the canyon causes an inshore excursion of the geostrophic shelf break current, and flow also enters the canyon across the canyon wall at the mouth slope. Some flow exits the canyon where the canyon and shelf intersect, but flow within the strait is strong and an inflow. The net transport along the canyon and the flow within the canyon are toward the left of the shelf break current in the northern hemisphere.

Appendix: Solving the System of Partial Differential Equations

As an example we present the solution procedure for the system of first-order partial differential equations (22) for $f > 0$. For $f < 0$ the process is similar. Substituting (22a) and (22c) into (22b) and (22d), the system reduces to

$$\left[\left(\frac{H_2}{g}\right)^{1/2}\coth\beta+\left(\frac{H_1}{g}\right)^{1/2}\right]A_t(y,t)-\left(\frac{H_2}{g}\right)^{1/2}\frac{1}{\sinh\beta}D_t(y,t)$$
$$-(H_2-H_1)A_y(y,t)=-(H_2-H_1)\eta_{Iy}, \tag{A1a}$$

$$-\left(\frac{H_2}{g}\right)^{1/2}\frac{1}{\sinh\beta}A_t(y,t)+\left[\left(\frac{H_2}{g}\right)^{1/2}\coth\beta+\left(\frac{H_1}{g}\right)^{1/2}\right]D_t(y,t)$$
$$+(H_2-H_1)D_y(y,t)=(H_2-H_1)\eta_{Iy}. \tag{A1b}$$

Define

$$a_{11}=a_{22}=\left(\frac{H_2}{g}\right)^{1/2}\coth\beta+\left(\frac{H_1}{g}\right)^{1/2}, \tag{A2a}$$

$$a_{12}=a_{21}=-\left(\frac{H_2}{g}\right)^{1/2}\frac{1}{\sinh\beta}, \tag{A2b}$$

$$b_{11}=-b_{22}=-(H_2-H_1), \tag{A2c}$$

$$h_1=-h_2=-(H_2-H_1)\eta_{Iy}(y), \tag{A2d}$$

and let $t=t(\psi)$ and $y=y(\psi)$, where ψ is a reference variable, so $A=A(\psi)$ and $D=D(\psi)$. Equation (A1) then collapses to

$$(b_{11}\dot{t}-a_{11}\dot{y})A_y-a_{12}\dot{y}D_y=h_1\dot{t}-a_{11}\dot{A}-a_{12}\dot{D}, \tag{A3a}$$

$$a_{12}\dot{y}A_y+(b_{11}\dot{t}+a_{11}\dot{y})D_y=h_1\dot{t}+a_{12}\dot{A}+a_{11}\dot{D}. \tag{A3b}$$

where the overdot denotes the derivative with respect to ψ.

The characteristic directions are given by

$$\begin{vmatrix} b_{11}\dot{t}-a_{11}\dot{y} & -a_{12}\dot{y} \\ a_{12}\dot{y} & b_{11}\dot{t}+a_{11}\dot{y} \end{vmatrix}=0, \tag{A4a}$$

i.e.,

$$\dot{y}=\pm c_0\dot{t} \tag{A4b}$$

where the positive parameter c_0 is defined as

$$c_0=\frac{-b_{11}}{\left(a_{11}^2-a_{12}^2\right)^{1/2}}=\frac{g^{1/2}\left(H_2-H_1\right)}{\left(H_2+H_1+2\left(H_1H_2\right)^{1/2}\coth\beta\right)^{1/2}}$$

or, in terms of γ and β defined in section 3 and with $c_1=\left(gH_1\right)^{1/2}$,

$$c_0=c_1\frac{\left|\gamma^2-1\right|}{\left(\gamma^2+2\gamma\coth\beta+1\right)^{1/2}}. \tag{A5}$$

Equation (A5) is the group and phase speed of long canyon waves that was derived in section 3.

From (A4b), we know that the system (A3) is of hyperbolic type and the two sets of characteristics are

$$dy=-c_0dt, \text{ i.e., } y+c_0t=C1,$$

$$dy=c_0dt, \text{ i.e., } y-c_0t=C2$$

where $C1$ and $C2$ are constants. From (A4a) the coefficients of (A3a) and (A3b) must be in a constant ratio for a solution to exist. We define this ratio as χ, i.e.,

$$\frac{b_{11}\dot{t}-a_{11}\dot{y}}{a_{12}\dot{y}}=\frac{-a_{12}\dot{y}}{b_{11}\dot{t}+a_{11}\dot{y}}=\frac{h_1\dot{t}-a_{11}\dot{A}-a_{12}\dot{D}}{h_1\dot{t}+a_{12}\dot{A}+a_{11}\dot{D}}=\chi. \tag{A6}$$

Substituting (A2d) into (A6), we obtain

$$\left(\chi a_{12}+a_{11}\right)dA(y,t)+\left(\chi a_{11}+a_{12}\right)dD(y,t)$$

$$+\left(1-\chi\right)\left(H_2-H_1\right)\frac{dt}{dy}\,d\eta_I(y)=0. \tag{A7}$$

On a characteristic, $y+c_0t=C1$ (i.e., $dy=-c_0dt$), (A6) becomes

$$\chi_1=-\left(\frac{b_{11}+a_{11}c_0}{a_{12}c_0}\right), \tag{A8}$$

and (A7) becomes

$$\left(\chi_1a_{12}+a_{11}\right)dA(y,t)+\left(\chi_1a_{11}+a_{12}\right)dD(y,t)$$

$$-\left(1-\chi_1\right)\frac{H_2-H_1}{c_0}\,d\eta_I(y)=0. \tag{A9}$$

Integrating (A9), we have

$$\left(\chi_1a_{12}+a_{11}\right)A(y,t)+\left(\chi_1a_{11}+a_{12}\right)D(y,t)$$

$$-\left(1-\chi_1\right)\frac{H_2-H_1}{c_0}\,\eta_I(y)=C3 \tag{A10}$$

where $C3$ is a constant along a characteristic $y+c_0t=C1$.

Similarly, on a characteristic, $y-c_0t=C2$ (i.e., $dy=c_0dt$), (A6) becomes

$$\chi_2=\frac{b_{11}-a_{11}c_0}{a_{12}c_0}, \tag{A11}$$

and similar to (A10), we have

$$\left(\chi_2a_{12}+a_{11}\right)A(y,t)+\left(\chi_2a_{11}+a_{12}\right)D(y,t)$$

$$+\left(1-\chi_2\right)\frac{H_2-H_1}{c_0}\,\eta_I(y)=C4 \tag{A12}$$

where $C4$ is a constant along a characteristic $y-c_0t=C2$.

Because on each characteristic $y+c_0t=C1$, the left-hand side of (A10) is a constant $C3$, and on each characteristic $y-c_0t=C2$, the left-hand side of (A12) is a constant $C4$, let these two constants be

$$C3=-\left(\frac{H_2-H_1}{c_0}\right)\left(1-\chi_1\right)W_p(y+c_0t),$$

$$C4=\frac{H_2-H_1}{c_0}\left(1-\chi_2\right)W_n(y-c_0t),$$

where W_n and W_p are arbitrary functions of one variable and are related to the information carried along the characteristics (see section 4.1). Then

$$\left(\chi_1a_{12}+a_{11}\right)A(y,t)+\left(\chi_1a_{11}+a_{12}\right)D(y,t)$$

$$=\frac{-\left(H_2-H_1\right)\left(1-\chi_1\right)}{c_0}\left[W_p(y+c_0t)-\eta_I(y)\right] \tag{A13a}$$

$$\left(\chi_2a_{12}+a_{11}\right)A(y,t)+\left(\chi_2a_{11}+a_{12}\right)D(y,t)$$

$$=\frac{\left(H_2-H_1\right)\left(1-\chi_2\right)}{c_0}\left[W_n(y-c_0t)-\eta_I(y)\right]. \tag{A13b}$$

It is straightforward to solve this system. Substituting (A8), (A11), (A2a), and (A2b) into (A13), and defining a parameter found in the process

$$\sigma=1-\left(\frac{a_{11}+a_{12}}{a_{11}-a_{12}}\right)$$

$$=1-\left(\frac{\left(H_2\right)^{1/2}\cosh\beta+\left(H_1\right)^{1/2}\sinh\beta-\left(H_2\right)^{1/2}}{\left(H_2\right)^{1/2}\cosh\beta+\left(H_1\right)^{1/2}\sinh\beta+\left(H_2\right)^{1/2}}\right)^{1/2},$$

or, in terms of γ and β,

$$\sigma(\gamma,\beta)=1-\left[\frac{\gamma\left(\cosh\beta-1\right)+\sinh\beta}{\gamma\left(\cosh\beta+1\right)+\sinh\beta}\right]^{1/2},$$

we obtain the solution of (A13) as (24) in the terms $W_p(y+c_0t)$ and $W_n(y-c_0t)$.

Acknowledgments. We are very grateful for the suggestions from referees on our first draft and to R. Thomson for suggestions on X. C.'s thesis which were incorporated here. This project was supported by a Department of Fisheries and Oceans/NSERC subvention and an NSERC research grant.

References

Abramowitz, M., and I. A. Stegun (Eds.), *Handbook of Mathematical Functions*, 1046 pp., Dover, Mineola, New York, 1968.

Allen, S. E., Rossby adjustment over a slope, Ph.D. thesis, 206 pp., Univ. of Cambridge, England, 1988.

Allen, S. E., Rossby adjustment over a slope in a homogeneous fluid, *J. Phys. Oceanogr.*, in press, 1996a.

Allen, S. E., Topographically generated, subinertial flows within a finite length canyon, *J. Phys. Oceanogr.*, in press, 1996b.

Cannon, G. A., Wind effects on currents observed in Juan de Fuca Submarine Canyon, *J. Phys. Oceanogr.*, *2*, 281-285, 1972.

Chen, X., Rossby adjustment over canyons, Ph.D. thesis, 278 pp., Univ. of B.C., Vancouver, Canada, 1996.

Crawford, W. R., W. S. Huggett, M. J. Woodward, and P. E. Daniel, Summer circulation of the waters in Queen Charlotte Sound, *Atmos. Ocean*, *23*, 393-413, 1985.

Drake, D. E., P. G. Hatcher, and G. H. Keller, Suspended particulate deposition in upper Hudson Submarine Canyon. In: *Sedimentation in Submarine Canyons, Fans and Trenches*, edited by K. J. Stanley and G. Kelling, pp. 33-41, Van Nostrand Reinhold, New York, 1978.

Foreman, M. G. G., Numerical model results for the west coast of Vancouver Island, in La Perouse Project Seventh Annual Report

1991, DFO Special Report, pp. 29-32, Dep. of Fish and Oceans, Inst. of Ocean Sci., Patricia Bay, B.C., Canada, 1992.

Freeland, H. J., and K. L. Denman, A topographically controlled upwelling center off southern Vancouver Island, *J. Mar. Res.*, *40*, 1069-1093, 1982.

Freeland, H. J., W. R. Crawford, and R. E. Thomson, Currents along the Pacific coast of Canada, *Atmos. Ocean*, *22*, 151-172, 1984.

Gill, A. E., *Atmosphere-Ocean Dynamics*, 662 pp., Academic Press, San Diego, Calif., 1982.

Gill, A. E., M. K. Davey, E. R. Johnson, and P. F. Linden, Rossby adjustment over a step. *J. Mar. Res.*, *44*, 713-738, 1986.

Gordon, R. L., and N. F. Marshall, Submarine canyons: Internal wave traps?, *Geophys. Res. Lett.*, *3*, 622-624, 1976.

Han, G. C., D. V. Hansen, and J. A. Galt, Steady-state diagnostic model of the New York Bight, *J. Phys. Oceanogr.*, *10*, 1998-2020, 1980.

Hickey, B., E. Baker, and N. Kachel, Suspended particle movement in and around Quinault Submarine Canyon, *Mar. Geol.*, *71*, 35-83, 1986.

Hotchkiss, F. L., and C. Wunsch, Internal waves in Hudson Canyon with possible geological implications, *Deep Sea Res.*, *29*, 415-442, 1982.

Hunkins, K., Mean and tidal currents in Baltimore Canyon, *J. Geophys. Res.*, *93*, 6917-6929, 1988.

Inman, D. L., C. E. Nordstrom, and R. E. Flick, Currents in submarine canyons: An air-sea-level interaction. *Annu. Rev. Fluid Mech.*, *8*, 275-310, 1976.

Keller, G. H., D. Lambert, G. Rowe, and N. Staresinic, Bottom currents in Hudson Canyon, *Science*, *180*, 181-183, 1973.

Keller, G. H., and F. P. Shepard, Currents and sedimentary processes in submarine canyons off the northeast United States, in: *Sedimentation in Submarine Canyons, Fans and Trenches*, edited by K. J. Stanley and G. Kelling, pp. 15-32, Van Nostrand Reinhold, New York, 1978.

Klinck, J. M., The influence of a narrow transverse canyon on initially geostrophic flow, *J. Geophys. Res.*, *93*, 509-515, 1988.

Klinck, J. M., Geostrophic adjustment over submarine canyons, *J. Geophys. Res.*, *94*, 6133-6144, 1989.

Mayer, D. A., G. C. Han, and D. V. Hanson, Circulation in the Hudson Shelf Valley: MESA physical oceanographic studies in New York Bight, *J. Geophys. Res.*, *87*, 9563-9578, 1982.

Press, W. H., B. P. Flannery, S. A. Teukolsky, and W. T. Vetterling, *Numerical Recipes- The Art of Scientific Computing*, 818 pp., Cambridge Univ. Press, New York, 1986.

Rhines, P. B., Slow oscillations in an ocean of varying depth, I, Abrupt topography, *J. Fluid Mech.*, *37*, 161-189, 1969.

Shepard, F. P., N. F. Marshall, P. A. McLoughlin, and G. G. Sullivan, Currents in submarine canyons and other sea valleys, *AAPG Stud. Geol.*, *8*, 173 pp., 1979.

Thomson, R.E., B. M. Hickey, and P. H. LeBlond, The Vancouver Island Coastal Current: Fisheries barrier and conduit, In *Effects of Ocean Variability on Recruitment and an Evaluation of Parameters Used in Stock Assesssment Models*, edited by R. Beamish and G. McFarlane, 265-296, *Spec. Publ. Fish. Aquat. Sci.*, *108*, 1989.

S.E. Allen and X. Chen, Oceanography, Department of Earth and Ocean Sciences, University of British Columbia, 6270 University Boulevard, Vancouver, British Columbia, Canada V6T 1Z4. (e-mail: allen@ocgy.ubc.ca)

(Received March 14, 1994; revised March 26, 1996; accepted April 11, 1996.)